Article

Immunity

Chimeric Antigen Receptor Designed to Prevent Ubiquitination and Downregulation Showed Durable Antitumor Efficacy

Graphical Abstract

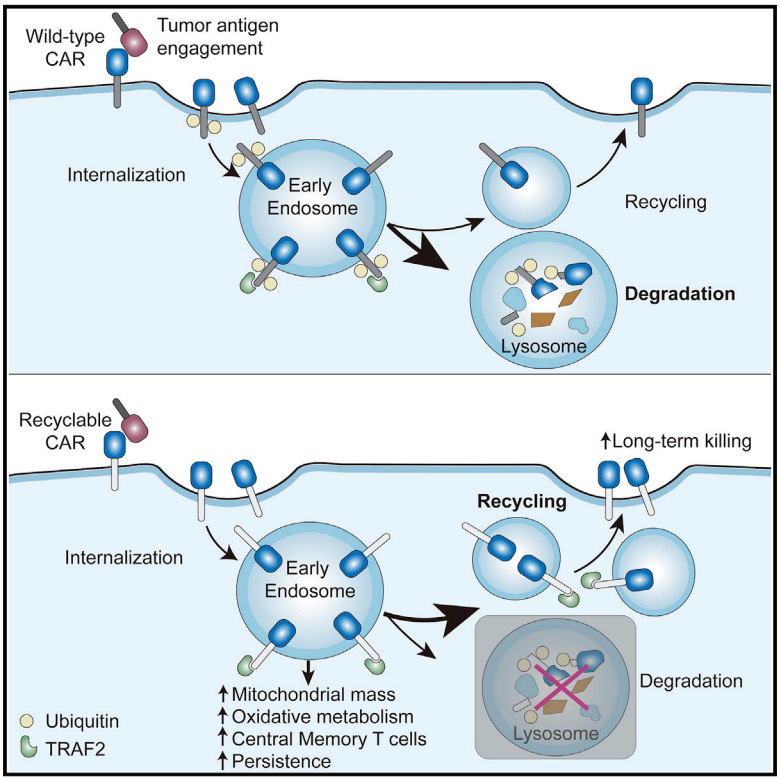

Highlights

- Tumor antigen encounter triggers CAR ubiquitination and downmodulation
- Tumor antigen-induced CAR ubiquitination targets CARs for lysosomal degradation
- CAR signaling in CAR-T cells expressing 4-1BB can be propagated in endosomes
- Blocking CAR ubiquitination enhances endosomal CAR signaling and CAR-T persistence

Authors

Wentao Li, Shizhen Qiu, Jian Chen, ..., Haitao Wu, Chenqi Xu, Haopeng Wang

Correspondence

eentwuhaitao@163.com (H.W.), cqxu@sibcb.ac.cn (C.X.), wanghp@shanghaitech.edu.cn (H.W.)

In Brief

Chimeric antigen receptor-T cell therapy offers a promising approach for cancer immunotherapy, but poor CAR-T persistence in patients limits therapeutic efficacy. Li et al. investigated the trafficking of CARs during CAR-T cell activation and designed a recyclable CAR with enhanced persistence and sustained antitumor function.

Li et al., 2020, Immunity *53*, 456–470
August 18, 2020
https://doi.org/10.1016/j.immuni.2020.07.011

CellPress

CellPress

Immunity

Article

Chimeric Antigen Receptor Designed to Prevent Ubiquitination and Downregulation Showed Durable Antitumor Efficacy

Wentao Li,[1,2,3,8] Shizhen Qiu,[1,8] Jian Chen,[4,8] Shutan Jiang,[2] Wendong Chen,[5] Jingwei Jiang,[1,2] Fei Wang,[1,2] Wen Si,[6] Yilai Shu,[4] Ping Wei,[6] Gaofeng Fan,[1] Ruijun Tian,[5] Haitao Wu,[4,*] Chenqi Xu,[2,7,*] and Haopeng Wang[1,9,*]

[1]School of Life Science and Technology, ShanghaiTech University, Shanghai 201210, China

[2]State Key Laboratory of Molecular Biology, CAS Center for Excellence in Molecular Cell Science, Shanghai Institute of Biochemistry and Cell Biology, Chinese Academy of Sciences, Shanghai 200031, China

[3]University of Chinese Academy of Sciences, Beijing 100049, China

[4]ENT institute and Department of Otorhinolaryngology, Eye & ENT Hospital, Fudan University, Shanghai 200031, China

[5]Department of Chemistry, Southern University of Science and Technology, Shenzhen 518055, China

[6]Center for Quantitative Biology and Peking-Tsinghua Joint Center for Life Sciences, Academy for Advanced Interdisciplinary Studies, Peking University, Beijing 100871, China

[7]School of Life Science, Hangzhou Institute for Advanced Study, University of Chinese Academy of Sciences, Hangzhou 310024, China

[8]These authors contributed equally

[9]Lead Contact

*Correspondence: eentwuhaitao@163.com (H.W.), cqxu@sibcb.ac.cn (C.X.), wanghp@shanghaitech.edu.cn (H.W.)

https://doi.org/10.1016/j.immuni.2020.07.011

SUMMARY

Clinical evidence suggests that poor persistence of chimeric antigen receptor-T cells (CAR-T) in patients limits therapeutic efficacy. Here, we designed a CAR with recyclable capability to promote *in vivo* persistence and to sustain antitumor activity. We showed that the engagement of tumor antigens induced rapid ubiquitination of CARs, causing CAR downmodulation followed by lysosomal degradation. Blocking CAR ubiquitination by mutating all lysines in the CAR cytoplasmic domain (CAR^{KR}) markedly repressed CAR downmodulation by inhibiting lysosomal degradation while enhancing recycling of internalized CARs back to the cell surface. Upon encountering tumor antigens, CAR^{KR}-T cells ameliorated the loss of surface CARs, which promoted their long-term killing capacity. Moreover, CAR^{KR}-T cells containing 4-1BB signaling domains displayed elevated endosomal 4-1BB signaling that enhanced oxidative phosphorylation and promoted memory T cell differentiation, leading to superior persistence *in vivo*. Collectively, our study provides a straightforward strategy to optimize CAR-T antitumor efficacy by redirecting CAR trafficking.

INTRODUCTION

Chimeric antigen receptor T cell (CAR-T cell) therapy has shown efficacy in treating hematological malignancies (Maude et al., 2014; Neelapu et al., 2017; Park et al., 2018; Schuster et al., 2017). However, as more data of CAR-T clinical trials are becoming available, current CAR-T therapy has shown some limitations. Recent studies reported that about 10%–20% of B cell malignancy patients failed to achieve complete remission (CR) after the CD19 CAR-T therapy and that approximately 30%–50% of patients who initially achieved complete remission had relapse of their cancer, mostly within 1 year after infusion of their CAR-T cells (Maude et al., 2018; Park et al., 2018). Furthermore, most patients with solid tumors have had no significant benefit from CAR-T therapy (Ahmed et al., 2015; Lamers et al., 2006; Schmidts and Maus, 2018; Watanabe et al., 2018). A major obstacle to the development of long-term effective CAR-T therapy is poor T cell persistence after infusion into patients. CAR-T cell *in vivo* persistence significantly correlates with ongoing disease-free survival in both acute and chronic lymphocytic leukemia (ALL and CLL, respectively) patients (Porter et al., 2015). Persistence of CAR-T cells plays an important role in mediating tumor regression, and poor T cell persistence was observed in several CAR-T trials with limited overall efficacy (Jensen et al., 2010; Kershaw et al., 2006; Lamers et al., 2005). Therefore, a better understanding of the molecular mechanism(s) controlling the persistence of CAR-T cells should lead to the development of more effective CAR-T therapy.

A common feature of antigen receptors (e.g., T cell receptor [TCR]) is ligand-induced downmodulation that is considered a hallmark of lymphocyte activation and one of the major mechanisms to regulate lymphocyte function (Liu et al., 2000). TCR downmodulation is mainly regulated by its ubiquitination induced by antigen stimulation (Wang et al., 2010a). Repressing

TCR ubiquitination leads to impaired TCR downmodulation as well as enhanced T cell response and effector function (Naramura et al., 2002; Yang et al., 2016). CAR is a synthetic antigen receptor targeting T cells to specifically kill tumor cells (Watanabe et al., 2018). Accumulating evidence suggests that CARs also undergo rapid downmodulation after engaging tumor antigens (Caruso et al., 2015; Davenport et al., 2015; Eyquem et al., 2017; Hamieh et al., 2019; Walker et al., 2017). However, the relationship between CAR-T efficacy and the dynamics of CAR expression after tumor antigen stimulation remains controversial. On the one hand, it is reported that effective internalization and re-expression of the CAR following antigen stimulation empowered by targeting of a CAR to the TCR α constant locus enhances CAR-T antitumor activity, suggesting that effective CAR downmodulation may be required for optimal CAR-T function (Eyquem et al., 2017). On the other hand, it has been suggested that CAR downmodulation might attenuate tumor killing ability of CAR-T cells following long-term tumor antigen engagement (Davenport et al., 2015). Mackall and colleagues also demonstrated that tumor antigen-induced CAR downmodulation was a limiting factor of CAR-T functionality and that nearly complete downmodulation of CAR within tumor microenvironment leads to limited antitumor efficacy in a solid tumor model (Walker et al., 2017). These results suggest that manipulation of CAR downmodulation may promote CAR-T efficacy. Thus, the prevention of CAR downmodulation may lead to more effective CAR-T therapy.

In this study, the following questions were addressed. (1) After CAR downmodulation, what is the fate of internalized CARs? (2) Do CARs undergo ubiquitination after ligand engagement, and how does this affect CAR downmodulation? (3) Does CAR ubiquitination and/or downmodulation contribute to the antitumor efficacy of CAR-T therapy? If so, can we design a new type of CAR by manipulating CAR ubiquitination? We found that tumor antigen encounter triggered rapid CAR ubiquitination, leading to CAR lysosomal degradation and downmodulation. Moreover, CAR-T cell persistence and functionality could be optimized by blocking this process.

RESULTS

Engagement of Tumor Antigens Induces CAR Downmodulation and Lysosomal Degradation

The CARs employed in our studies contain a single-chain variable fragment (scFv) that recognizes CD19 (unless otherwise indicated), CD8α stalk, and CD3ζ signal transduction domain (19ζ CAR). Some CARs also include a costimulatory domain derived from either CD28 (1928ζ CAR) or 4-1BB (19BBζ CAR) (Figure S1A). To investigate the mechanism that regulates CAR surface expression upon tumor antigen engagement, we first co-cultured primary 19ζ CAR-T cells with K562 myelogenous leukemia cells with ectopic expression of its tumor antigen, CD19, or a control antigen, mesothelin. Surface CAR expression on primary T cells was decreased by 80% after encountering tumor antigen, but not control antigen (Figure 1A, left). Similar results were also observed on 19ζ CAR-expressing Jurkat T cells (Figure 1A, middle, and Figure S1B). We further tested whether CAR downmodulation occurred in the tumor microenvironment *in vivo*. $CD19^+$ K562 cells were subcutaneously xenografted in NOD *scid Il2rg*$^{-/-}$ (NSG) mice, and primary 19ζ CAR-T cells were injected into these tumor-bearing mice. Consistent with the *in vitro* result, we observed marked downregulation of CAR expression on tumor-infiltrated CAR-T cells compared with that on CAR-T cells in the spleen from the same mice (Figure 1A, right). These results suggest that local antigen encounter in the tumor induces efficient downmodulation of surface CAR expression.

To further test whether the loss of CAR expression can revert back to the initial expression level once tumor antigen is removed, we first co-incubated CD19 CAR-T cells with $CD19^+$ tumor cells for 12 h, which resulted in a significant loss of surface CAR expression. We then sorted and replated these CAR-T cells in the presence or absence of $CD19^+$ tumor cells. We found that surface CAR expression was fully recovered after an additional 24 h culture in media, whereas surface CAR expression remained low in those T cells incubated again with $CD19^+$ tumor cells (Figure S1C). These results demonstrate that the downmodulation of CAR expression depends on the presence of tumor antigen.

Previous studies have suggested that TCR:CD3 complexes are downmodulated and targeted to lysosomes for degradation after antigen engagement (Liu et al., 2000; Wang et al., 2010a). To investigate whether downmodulated CARs are also degraded in lysosomes, we first assessed the protein amount of the CAR by using immunoblotting and intracellular staining. The total amount of CAR was significantly reduced after activation (Figures 1B and 1C). To determine the fate of internalized CAR, the stimulated CAR-T cells were treated with MG132, a 26S proteasome inhibitor, or NH_4Cl, which block lysosomal acidification and function. The treatment of MG132 resulted in an increased amount of total ubiquitinated protein in cells, whereas the treatment of NH_4Cl caused accumulation of p62 protein, an autophagy-lysosome adaptor protein, suggesting the effective inhibition of proteasomal and lysosomal degradation, respectively (Figure S1D). We found that lysosomal inhibition, but not proteasomal inhibition, largely blocked the degradation of CAR (Figure 1C). We further analyzed the intracellular location of the CAR by confocal microscopy using a GFP-fused CAR and the lysosome tracker. We observed that a substantial proportion of intracellular CARs appeared to colocalize with lysosomes in the activated CAR-T cells, but not resting CAR-T cells (Figures 1D and S1E). Taken together, these data suggest that CARs are downmodulated and targeted for lysosomal degradation after tumor antigen encounter.

CAR-T Activation Induces Rapid Ubiquitination of CAR, and Blocking of CAR Ubiquitination Redirects Its Trafficking

Ubiquitination of receptors is involved in ligand-induced receptor downmodulation and degradation (Acconcia et al., 2009; Haglund and Dikic, 2005; Hicke and Dunn, 2003; Hicke and Riezman, 1996). Our previous study has demonstrated that ubiquitination of TCR:CD3 complex in immature T cells triggers TCR downmodulation (Wang et al., 2010a). Therefore, we speculated that CAR activation after tumor antigen engagement may trigger ubiquitination of CAR. To test this possibility, 19ζ CAR-T cells were co-incubated with $CD19^+$ target cells for 60 min, and the amount of CAR ubiquitination was assessed at different time

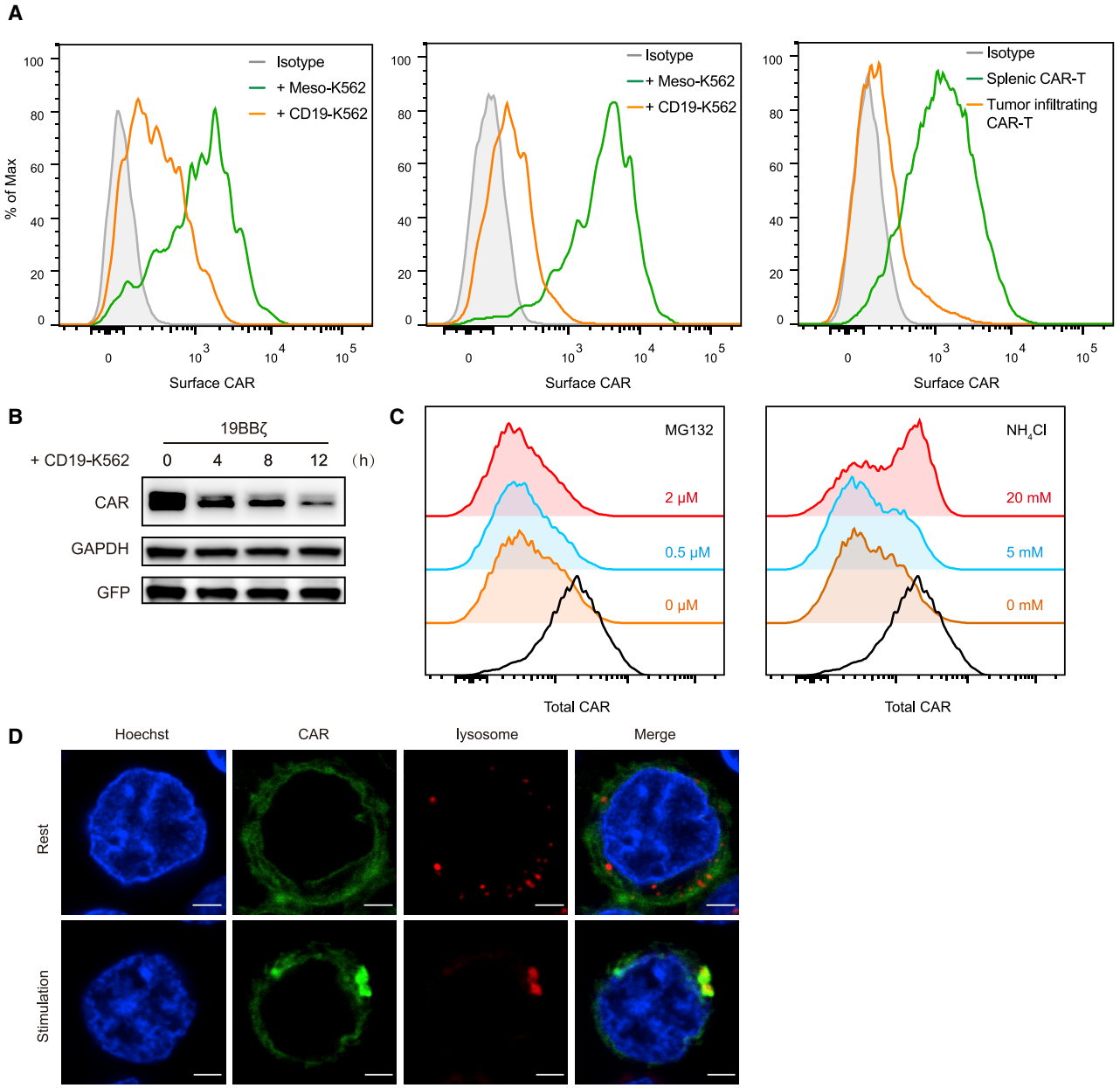

Figure 1. Engagement of Tumor Antigens Induces CAR Downmodulation and Lysosomal Degradation

(A) FACS analysis of surface CAR expression level. 19ζ CAR-expressing human T cells (left) or Jurkat cells (middle) were co-incubated with $CD19^+$ K562 cells or $Meso^+$ K562 cells overnight. 2 weeks after transferring into tumor-bearing mice, the CAR-T cells were isolated from the spleen and the tumor for FACS analysis (right). See also Figure S1.

(B) Immunoblot analysis of total CAR protein level during CAR-T cell activation.

(C) FACS analysis of total CAR level. CAR-T cells were co-incubated with $CD19^+$ K562 cells in the presence of MG132 or NH_4Cl. Total CAR level was measured using intracellular FACS analysis. Black line represents unstimulated CAR-T cells.

(D) Representative images of CAR (fused with GFP) and lysosomes (stained with LysoTracker). Scale bars, 2.5 μm. See also Figure S1.

All experiments were independently repeated at least three times.

points. We found that tumor antigen stimulation triggered rapid ubiquitination of the CAR, which was already detectable at 2 min of stimulation, peaked at 5–10 min, and decreased to basal level within 60 min (Figure 2A). We next tested whether blocking this CAR ubiquitination would affect CAR downmodulation and degradation. Our previous study has shown that all intracellular lysines of CD3 chains are required to mediate TCR:CD3 ubiquitination after T cell activation (Wang et al., 2010a). Consistently, our mass spectrometry analysis revealed that most of the intracellular lysine residues of either a 19BBζ CAR or a 1928ζ CAR

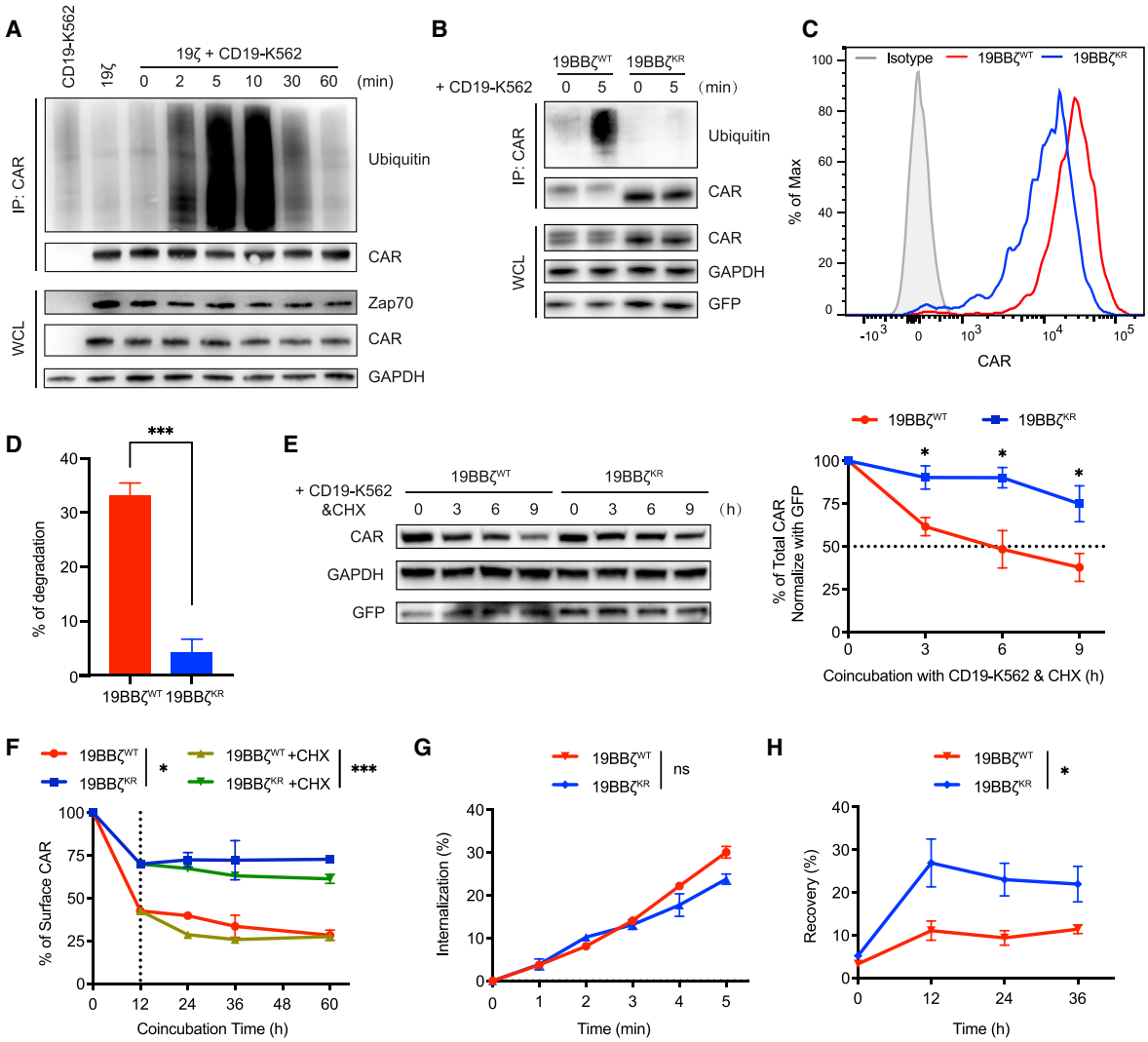

Figure 2. Tumor Antigens Trigger Ubiquitination of the CAR, and Blocking of CAR Ubiquitination Redirects Its Trafficking

(A) Immunoblot analysis of CAR ubiquitination. Jurkat cells expressing 19ζ CAR were co-incubated with $CD19^+$ K562 cells for indicated time. CAR proteins were immunoprecipitated by anti-Myc beads and separated by SDS–PAGE, and western blots were probed with anti-Ubiquitin antibody (Ab) and anti-Myc Ab. The protein levels of ZAP-70, CAR, and GAPDH in the whole-cell lysate were analyzed by western blot.

(B) Immunoblot analysis of CAR ubiquitination in $19BB\zeta^{WT}$ CAR-T cells and $19BB\zeta^{KR}$ CAR-T cells. See also Figure S2.

(C) FACS analysis of surface CAR expression level on $19BB\zeta^{WT}$ CAR-T cells and $19BB\zeta^{KR}$ CAR-T cells.

(D) FACS-based CAR degradation analysis in primary CAR-T cells. Total CAR level was examined using intracellular FACS analysis, and mean fluorescence intensity was obtained to calculate percentage of degradation.

(E) Immunoblot analysis of total CAR protein level in activated CAR-T cells. Primary CAR-T cells were co-incubated with $CD19^+$ K562 cells for indicated time in the presence of 10 μg/mL CHX. Total CAR level was detected by immunoblotting analysis. Representative western blot (left) and quantification of CAR level normalized by GFP level (right, n = 3) were shown.

(F) FACS analysis of surface CAR expression level. $19BB\zeta^{WT}$ and $19BB\zeta^{KR}$ CAR-T cells were co-incubated with $CD19^+$ K562 cells for indicated time. CHX (100 μM) was added into the culture medium 12 h post activation. The surface CAR level was normalized to the basal CAR expression level. See also Figure S2.

(G) FACS analysis of CAR internalization rate. CAR-T cells were treated with BFA (10 μg/mL) in 37°C for indicated time. The surface CAR level was then measured by FACS analysis, and the level of internalized CAR was normalized to basal CAR expression level.

(H) FACS analysis of recycling of internalized CAR. After co-incubating with target cells for 12 h, CAR-T cells were treated with proteinase K (0.1 mg/mL) to remove noninternalized CAR on cell surface and then replated in medium with CHX (100 μM). The increase of surface CAR expression level was monitored by FACS every 12 h.

All experiments were independently repeated at least three times. Error bars represent ± SEM (*$p < 0.05$, ***$p < 0.001$).

were ubiquitinated in resting CAR-T cells, and the ubiquitination level was further enhanced after CAR activation in both CAR-expressing Jurkat T cells and primary CAR-T cells (Tables S1 and S2). To block CAR ubiquitination, we generated a new version of CAR (CAR^{KR}), in which all cytoplasmic lysines were mutated to arginines. As expected, activation-induced CAR ubiquitination was completely blocked in CAR^{KR}-T cells after antigen stimulation (Figures 2B and S2A). Surface expression of CAR^{KR} was

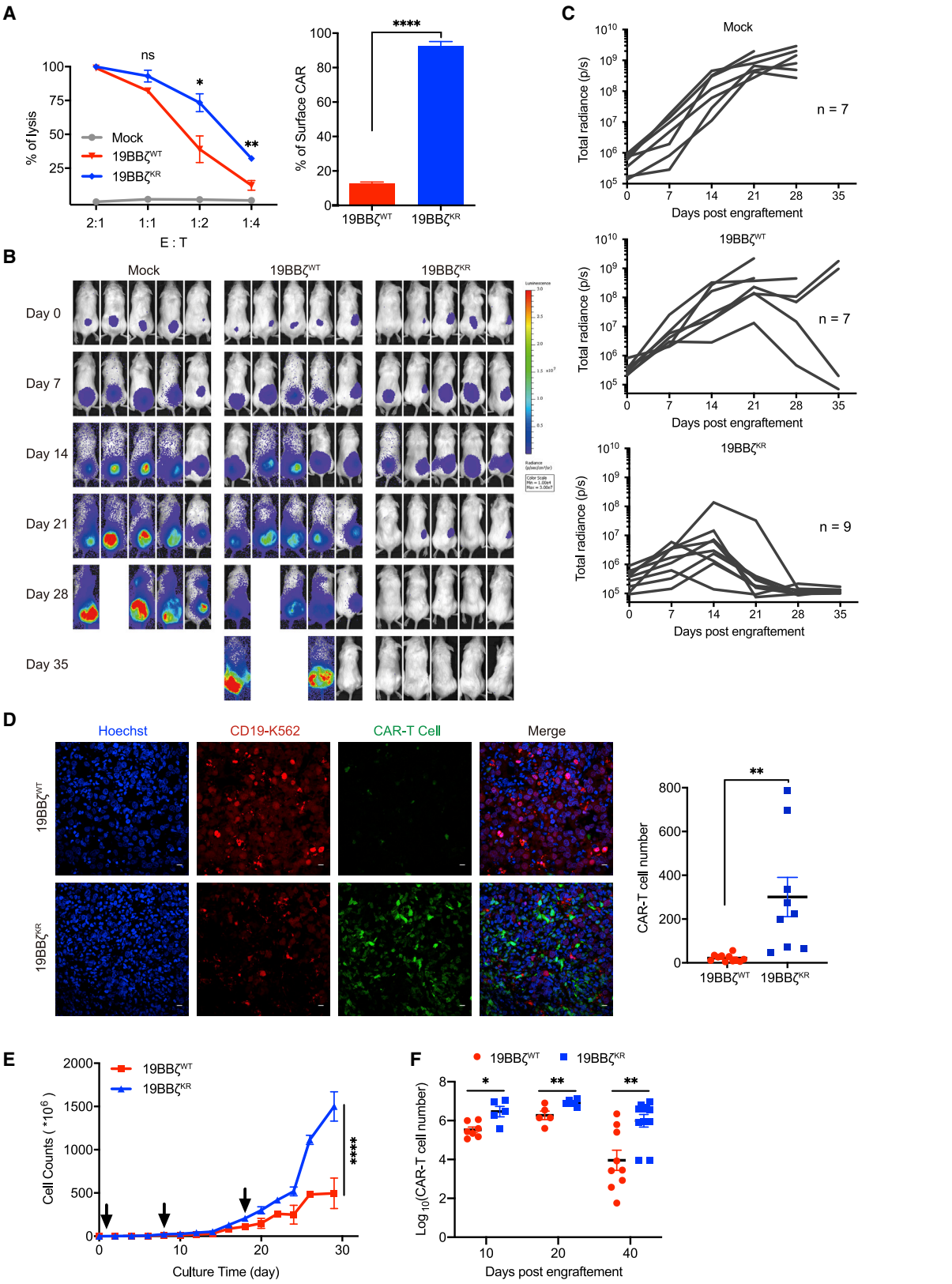

(legend on next page)

moderately reduced compared with wild-type CAR (CAR^{WT}) (Figure 2C), although both CARs were expressed at similar protein levels (Figures S2B and S2C). Of note, similar surface expression reduction was also reported in the case of TCR (Thien et al., 2003; Wang et al., 2010a).

We then tested whether CAR ubiquitination affected CAR degradation in the setting of CAR incorporating 4-1BB costimulation domain. Interestingly, the total level of CAR^{KR} remained largely unchanged after CAR activation, whereas over 30% of CAR^{WT} was degraded 1 h post CAR-T cell activation (Figure 2D). To exclude the possibility that CAR^{KR} might produce more newly synthesized CAR protein instead of inhibiting the turnover of the CAR protein, we treated the CAR-T cells with cycloheximide (CHX), a protein synthetic inhibitor, during CAR-T activation. While the CAR^{WT} exhibited a half-life of 6 h, CAR^{KR} remained about 75% of initial protein amount even after 9 h of CHX treatment (Figure 2E). Given the result that the activation-induced degradation of the CAR^{KR} was substantially reduced, we further compared the dynamics of surface expression of CAR^{WT} and CAR^{KR}. We found that the CAR downmodulation was significantly inhibited in CAR^{KR}-T cells compared with CAR^{WT}-T cells (Figures 2F and S2D). This was not due to more CAR mRNA transcribed or more newly synthesized CAR protein produced in CAR^{KR}-T cells than CAR^{WT}-T cells (Figures S2E and 2F). To test whether CAR ubiquitination regulates CAR surface expression independent of the type of CAR, we measured the kinetics of CAR downmodulation in setting of 28ζ CAR-specific targeting GD2 antigen (GD2-28ζ) (Figure S1A). Although different types of CAR exhibited distinct CAR downmodulation kinetics, the downmodulation of both CAR^{KR}s were substantially inhibited compared with CAR^{WT} (Figure S2F). These results demonstrated that CAR ubiquitination regulated CAR downmodulation and this regulation in an independent manner of scFvs and costimulatory domains of the CAR constructs.

The inhibition of CAR downmodulation in CAR^{KR}-T cells (Figure 2F) could be due to impaired CAR internalization or enhanced recycling of the internalized CAR back to the cell surface. To distinguish these two possibilities, we first assessed the internalization rate of both CAR^{WT} and CAR^{KR} in CAR-T cells. The internalization assay of CAR was performed as previously described (Liu et al., 2000). Brefeldin A (BFA) can induce fusion of early endosomes with the *trans*-Golgi network (TGN), and this property was exploited to study the internalization of CAR. BFA treatment resulted in the reduction of surface CAR expression, suggesting that CARs are continuously internalized from cell membrane. Importantly, we found that both CAR^{WT}-T cells and CAR^{KR}-T cells internalized their CARs at a comparable rate (Figure 2G). To further examine whether the internalized CARs return to cell surface in activated CAR-T cells and whether CAR^{KR} promotes this process, we first co-incubated the CD19 CAR-T cells with $CD19^+$ tumor cells for 12 h to ensure an efficient CAR downmodulation. Activated CAR-T cells were then treated with proteinase K, which efficiently removed the noninternalized CAR proteins on the cell surface (Figure S2G). These cells were cultured at 37°C again in the presence of CHX that blocks new synthesized CAR protein, and the recovery of surface CAR expression were measured at various time points. We found that there were markedly more internalized CAR^{KR} recycled back to the cell surface than CAR^{WT} (Figure 2H). Collectively, these data suggest that CAR ubiquitination regulates CAR downmodulation by preventing internalized CAR from being recycled back to the T cell surface and promoting their lysosomal degradation.

CAR^{KR}-T Outperforms CAR^{WT}-T *In Vivo*, Achieving Complete Tumor Eradication

We next sought to compare the cytotoxicity of CAR^{WT}-T and CAR^{KR}-T cells *in vitro*. In a standard 12 h cytotoxicity assay, 19BBζ CAR^{WT}-T and 19BBζ CAR^{KR}-T cells showed nearly equivalent tumor-killing ability (Figures S3A and S3B). The indistinguishable cytotoxicity was extended in their similar cytokine secretion capacity in both CD4 and CD8 CAR-T cells, suggesting that CAR^{KR} did not increase the risk of cytokine release syndrome (Figures S3C and S3D). Since a previous study has suggested that downmodulation of CAR may result in the impaired cytotoxicity of CAR-T cells in a long-term assay of killing (Davenport et al., 2015), we extended the time of the cytotoxicity assay to 3 days. In this prolonged cytotoxicity assay, CAR^{KR}-T cells were more effective killers than CAR^{WT}-T cells, especially at low effector-to-target ratios (less than 1:1), which is mimicking the condition of high tumor burden *in vivo* (Figure 3A, left). As expected, the downmodulation of CAR^{KR} was largely inhibited (Figure 3A, right). In addition, to rule out the possibility that the better killing capacity of the CAR^{KR}-T cells results from its moderately reduced basal surface expression, we sorted both CAR^{WT}-T and CAR^{KR}-T cell population with an equivalent basal surface CAR expression (Figure S3E). These sorted CAR^{KR}-T cells again showed more efficient killing capacity than the sorted CAR^{WT}-T cells in a 3-day tumor-killing assay (Figure S3F). Taken together,

Figure 3. 19BBζ CAR^{KR}-T Outperforms CAR^{WT}-T *In Vivo*, Achieving Complete Tumor Eradication

(A) *In vitro* cytotoxicity assay of CAR-T cells against $CD19^+$ K562 cells. Killing efficiency was analyzed by FACS (left). FACS analysis of the remaining surface CAR level at the end of *in vitro* cytotoxicity assay (right). n = 3, representative of three donors.

(B) Representative bioluminescence images of tumor growth over time.

(C) Tumor burden was quantified as the total photon count from luciferase intensity of each mouse by IVIS imaging. Each line represents one mouse, n = 7–9 mice per group.

(D) Representative images of CAR-T cells infiltrating in the tumor sites. 12 days after the transfer of CAR-T cells, the tumor samples in the right flank of NSG mice were harvested. Representative images of CAR-T cells infiltrating in the tumor sites are shown (left), GFP^+ CAR-T cells infiltrated in the tumor sections was quantitated by counting, and the average numbers of infiltrated CAR-T cells per reported field were calculated in random areas of the tumor samples (right). Nucleus stained with Hoechst (blue), $CD19^+$ K562-mCherry (red), and CAR-GFP (green) are shown. Scale bars, 10 μm. Representative of at least three mice.

(E) *In vitro* proliferation assay of 19BBζ^{WT} and 19BBζ^{KR} CAR-T cells. Cumulative cell counts of the CAR-T cells during serial stimulations by adding irradiated $CD19^+$ K562 cells. Arrows indicate time points of stimulating CAR-T cells with tumor cells. Representative of three donors.

(F) Number of CAR-T cells in the spleen of tumor-bearing mice at indicated post-infusion time. Each point represents one mouse, n = 5–11 mice per group. Error bars represent ± SEM (*p < 0.05, **p = < 0.01, ****p < 0.0001).

these data suggest that CAR^{KR}-T cells are more effective long-term killers than CAR^{WT}-T cells.

We next investigated the therapeutic efficacy of 19BBζ CAR^{KR}-T cells in an *in vivo* tumor model in which Luci-Red^{+} CD19^{+}K562 tumor cells were subcutaneously injected into the flank of NSG mice (Zhao et al., 2015). Tumor growth was monitored by quantitative imaging system every week. In contrast to the finding that most mice in CAR^{WT}-T-treated groups eventually succumbed to tumor, CAR^{KR}-T cells achieved durable and complete tumor eradication in all treated mice (Figures 3B and 3C). In accordance with this observation, CAR^{KR} promoted higher CAR-T cell accumulation at the tumor site relative to CAR^{WT} (Figure 3D). We further compared the cytotoxicity of two types of 19BBζ CAR-T cells *ex vivo* by isolating CAR-T cells from spleens of tumor-bearing mice. Consistent with *in vitro* observation, CAR^{KR}-T cells showed more efficient killing capacity than CAR^{WT}-T cells at low effector-to-target ratios (Figure S3G). Several studies support the notion that a proper lower CD4/CD8 ratio of adoptive T cells predicts better antitumor response (Radvanyi et al., 2012; Zhao et al., 2015). In our model, we indeed observed an increased CD8/CD4 ratio of CAR^{KR}-T cells after infusion (Figure S4A), which may be due to the fact that CAR^{KR} preferentially promotes the expansion of CD8^{+} CAR-T cells (Figures S4B and S4C). Taken together, these data demonstrated that 19BBζ CAR^{KR}-T cells outperformed the 19BBζ CAR^{WT}-T cells *in vivo*.

Since robust expansion and long-term persistence of CAR-T cells play an important role in effective tumor clearance, we next compared the proliferative capacity of CAR^{WT}-T and CAR^{KR}-T cells *in vitro*. 19BBζ CAR-T cells were expanded in response to three weekly stimulation with irradiated CD19^{+} target cells. Interestingly, CAR^{KR}-T cells exhibited more robust proliferation than CAR^{WT}-T cells (Figure 3E). To further assess the proliferation and persistence of CAR-T cells *in vivo*, splenic CAR-T cells in the tumor-bearing mice were enumerated 10, 20, and 40 days post CAR-T infusion (Figure 3F). As was seen in the *in vitro* proliferation assay, CAR^{KR}-T cells displayed superior initial expansion 10 days post infusion compared with CAR^{WT}-T cells (Figure 3F). Interestingly, the number of CAR^{WT}-T cells reached the peak on day 20 and diminished 40 days post T cell infusion. In contrast, CAR^{KR}-T cells displayed greater persistence, and there were over 100-fold more CAR^{KR}-T cells than CAR^{WT}-T cells on day 40. Consistently, the percentage of CAR^{KR} positive T cells was significantly more enriched than CAR^{WT} positive T cells in T cell population within spleen, blood, and tumor sites after infusion (Figure S4D). To further test whether the superior persistence of CAR^{KR}-T cells confers a long-lasting tumor protection, we re-challenged mice that had previously cleared their primary tumor with a second intravenous injection of tumor cells. CAR^{KR}-T cells, but not CAR^{WT}-T cells, completely protected mice against re-challenged tumor and survive for at least 120 days since the initial injection of tumor (Figure S4E). In summary, these data suggest that blocking CAR ubiquitination promotes *in vivo* persistence and antitumor activity of 19BBζ CAR-T cells.

Incorporating 4-1BB Motif, CAR^{KR} Promotes CAR-T Cell Differentiation toward Memory T Cells

Previous studies have shown that differentiation states of T cells determine their proliferative and survival capacities, which strongly correlate with antitumor potency of adoptive transferred T cells (Berger et al., 2008; Fraietta et al., 2018; Gattinoni et al., 2011). We therefore examined the differentiation states of CAR-T cells *in vivo* by using CD62L and CD45RA as the differentiation markers. We found that, compared with 19BBζ CAR^{WT}-T cells, 19BBζ CAR^{KR}-T cells exhibited a higher percentage of central memory cells (CD62L^{+}CD45RA^{-}, Tcm [T central memory]) and a decrease in the proportion of terminally differentiated effector cells (CD62L^{-}CD45RA^{+}, Teff [T effector] cell) in both CD8 T cells (Figures 4A and 4B) and CD4 T cells (Figure S5A) in the spleen as well as in T cells from the blood (Figure S5B). In addition, we assessed the expression of CD27 and CD45RO, which are also associated with Tcm cells. Consistent with the phenotype in spleen and blood, a higher proportion of Tcm cells (CD27^{+}CD45RO^{+}) was observed in tumor-infiltrated CAR^{KR}-T cells compared with CAR^{WT}-T cells (Figures 4C and 4D). We also examined the differentiation characteristics of *in vitro*-expanded CAR^{WT}-T and CAR^{KR}-T cells in response to stimulation with irradiated target cells. CAR^{KR}-T cells accumulated a higher fraction of Tcm cells than CAR^{WT}-T cells in both CD8 T cell subset (Figure 4E) and CD4 T cell subset (Figure S5C), agreeing with our *in vivo* results. Taken together, these data demonstrated that CAR^{KR} enhanced the accumulation of the central memory T cell populations.

CAR^{KR} Promotes 4-1BB-TRAF Interaction in Accumulated CAR-4-1BB Signaling Endosomes and Enhances Downstream NF-κB and mTOR Activities

Previous study has suggested that 4-1BB is a potent costimulatory signaling that promotes T cell proliferation and memory cell formation (Watts et al., 2011). In addition, 4-1BB motif in the CAR architecture promoted the outgrowth of CD8^{+} central memory T cells and enhanced CAR-T cell persistence (Kawalekar et al., 2016). Therefore, we hypothesize that the 4-1BB signaling may be specifically amplified in 19BBζ CAR^{KR}-T cells. The 4-1BB signal is mediated by engaging TRAF family proteins as scaffold proteins to recruit downstream molecules to activate the canonical nuclear factor κB (NF-κB), p38-MAPK, and mammalian target of rapamycin (mTOR) pathways (Kim et al., 2009; Menk et al., 2018; Teijeira et al., 2018; Zapata et al., 2018). Among the TRAF family proteins, TRAF2 is reported to play a key role in 4-1BB signaling in both T cells and CAR-T cell (Li et al., 2018; Saoulli et al., 1998). It has been demonstrated that 4-1BB agonist antibody stimulation triggers 4-1BB internalization, and interestingly, endocytosed 4-1BB molecules within the early endosomes recruit TRAF2 molecules that coat the cytoplasmic side of their surface. These 4-1BB containing early endosomes remain as an active signaling complex, constituting signaling endosomes (Martinez-Forero et al., 2013; Zapata et al., 2018). To compare the recruitment of TRAF2 to CAR^{WT} and CAR^{KR}, we conducted microscopy analysis to study the interaction between 19BBζ CAR receptor and TRAF2 protein in CAR-expressing Jurkat cells. After tumor antigen stimulation, CARs were internalized toward EEA1-marked early endosomal vesicles. Importantly, we found that most CAR-containing endosomes colocalized with TRAF2 proteins, indicating the internalized endosomal 19BBζ CAR receptors recruited cytosolic TRAF2 to constitute an active signaling complex (Figure 5A). Due to the impaired lysosomal degradation of internalized of CAR^{KR} (Figure 2E), about

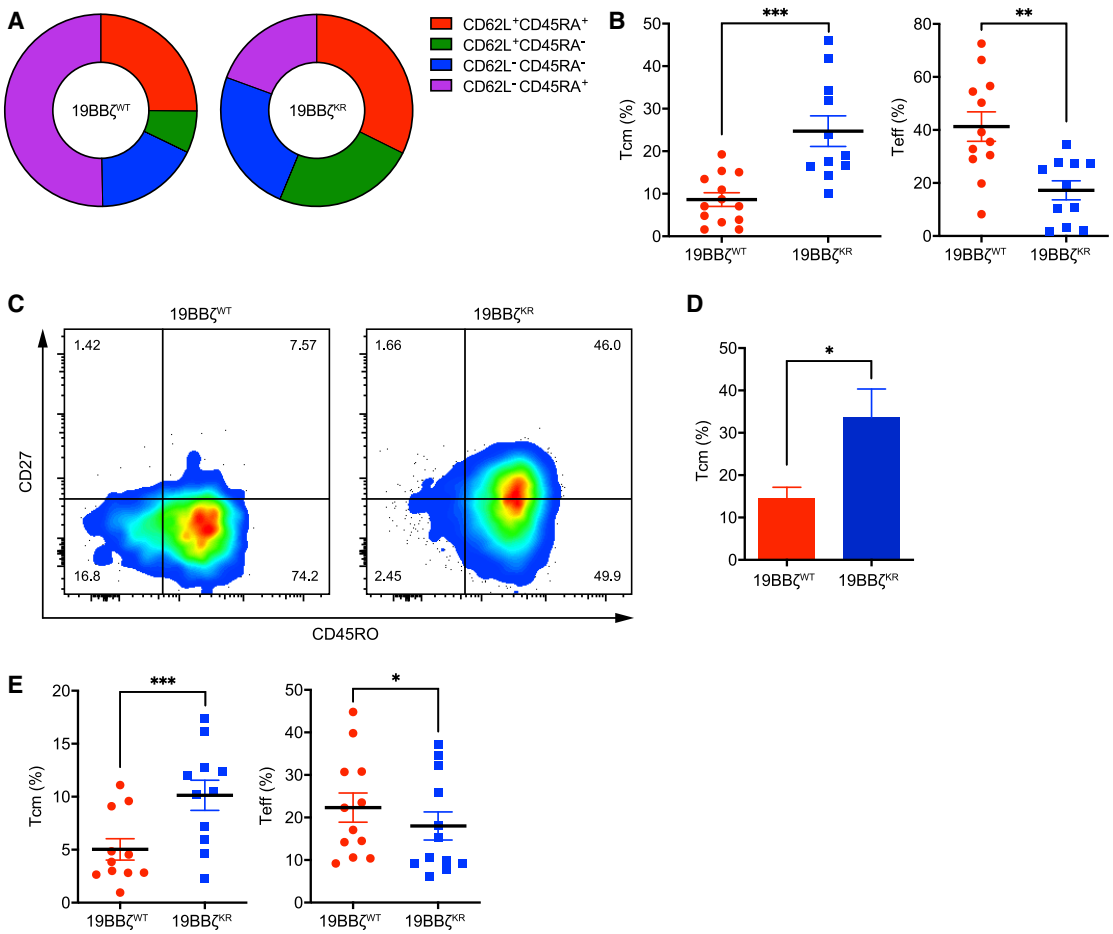

Figure 4. 19BBζ CAR^{KR} Promotes CAR-T Cell Differentiation toward Memory T Cells

(A) Representative CD62L/CD45RA-expressing profile in CD8$^+$ CAR-T cells from the spleen of tumor-bearing mice. Data are representative of 11 mice per group.

(B) FACS analysis of CD8$^+$ CAR-T cells in the spleen of tumor-bearing mice. Central memory cells (CD62L$^+$CD45RA$^-$) and terminal effector cells (CD62L$^-$CD45RA$^+$) are shown. Each point represents one mouse, n = 11–13 mice per group. See also Figure S5.

(C) Representative FACS plot of expression of CD27 and CD45RO on CAR-T cells isolated from the tumor sites 14 days post infusion.

(D) Percentage of CD27$^+$CD45RO$^+$ CAR-T cells in the tumor sites. n = 4 mice per group.

(E) FACS analysis of CD8$^+$ CAR-T cells stimulated with the irradiated CD19$^+$ K562 cells. Each point represents one independent experiment, n = 11. See also Figure S5.

Error bars represent ± SEM (*p < 0.05, **p < 0.01, ***p < 0.001).

2.5-fold more signaling endosomes were accumulated in CAR^{KR}-T cells compared with CAR^{WT}-T cells (Figures 5A and 5B). To further confirm this result, we biochemically purified and analyzed the early endosomes from CAR-T cells. We found that early endosomes from 19BBζ CAR-T cells, but not 1928ζ CAR-T cells, contained TRAF2 proteins, suggesting that TRAF2 is specifically recruited to 4-1BB domain of CAR (Figures 5C and S6A). Immunoblotting analysis of Rab5 protein, a marker of early endosomes, indicated that comparable amounts of endosomes were isolated from CAR^{WT}-T cells and CAR^{KR}-T cells. However, there were more CARs and TRAF2 proteins in the endosomes from CAR^{KR}-T cells than from CAR^{WT}-T cells, suggesting that blocking ubiquitination of 19BBζ CAR resulted in more CAR-TRAF2 signaling endosomes (Figure 5C).

To further study the signaling characteristics of CAR^{KR}, we compared the downstream binding partners of CAR^{WT} and CAR^{KR}. 19BBζ CARs were immunoprecipitated from both resting and activated primary CAR-T cells, and the interactions between CARs and their potential binding partners were measured (Figure 5D). There are two types of signaling proteins that can interact with CAR containing 4-1BB motif: CD3ζ-ITAM binding partners (e.g., ZAP-70) and 4-1BB binding partners (such as TRAF2 or THEMIS, a protein that was recently reported to be recruited to 4-1BB after CAR-T activation) (Sun et al., 2020). We found that comparable amount of ZAP-70 was recruited to both CAR^{WT} and CAR^{KR} after CAR-T cell activation. Consistently, the phosphorylation level of LAT, a substrate of ZAP-70 kinase, was similar in activated CAR^{WT}-T cells and CAR^{KR}-T cells. While no detectable p85 protein (a CD28 binding partner) was associated with either CAR^{WT} or CAR^{KR}, there were more 4-1BB binding partners, TRAF2 and THEMIS, interacting with CAR^{KR} than with CAR^{WT}. This result is consistent with our data in Figures 5A and 5B, which show that there are significantly more CAR-TRAF2 containing signaling endosomes in CAR^{KR}-T cells.

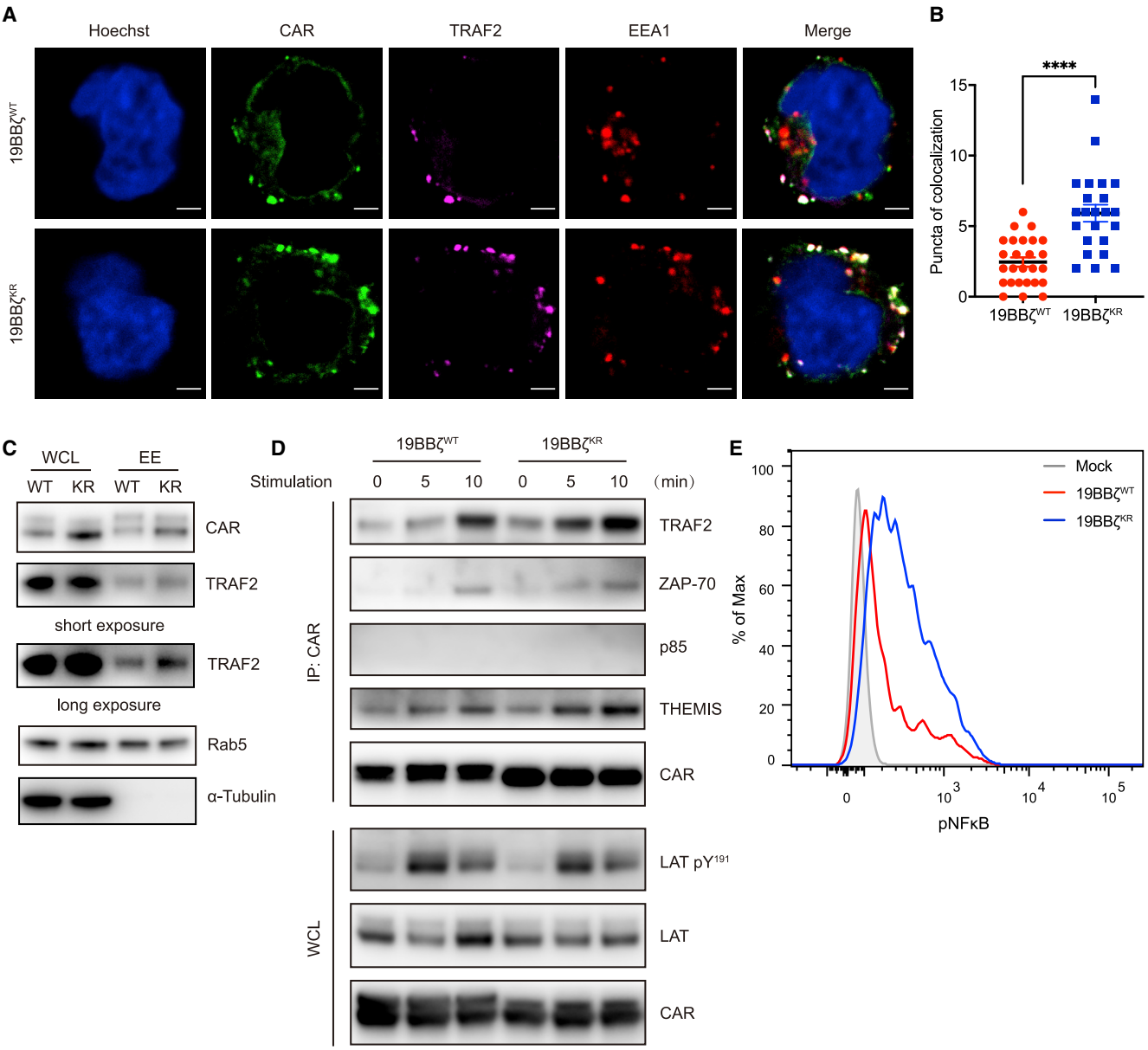

Figure 5. Accumulated CAR-4-1BB Signaling Endosomes in CAR^{KR}-T Cells Promote 4-1BB-TRAF Interaction and 4-1BB Signaling

(A) Imaging analysis of CAR, TRAF2, and EEA1 in CAR-T cells 60 min after stimulation. Hoechst (blue), CAR-fused EGFP (green), TRAF2-fused mCherry (pink), and EEA1 (red). Scale bars, 2 μm.

(B) Number of the puncta, in which CAR, TRAF2, and EEA1 were colocalized in (A). Data of at least 20 randomly chosen individual cells are shown and represented as mean ± SEM (****$p < 0.0001$).

(C) Immunoblot analysis of CAR and TRAF2 protein levels in the endosomes isolated from CAR-T cells. Immunoblotting analysis of Rab5 and α-Tubulin was performed to examine the purity of exaction of the early endosomes. WCL, whole cell lysate; EE, early endosome.

(D) BBζ CARs were immunoprecipitated from both resting and activated CAR-T cell lysates, separated by SDS–PAGE. Western blots were probed with antibodies against the indicated signaling proteins.

(E) FACS analysis of NF-κB phosphorylation level in CAR-T cells.

All data above acquired from at least three independent experiments.

We further studied whether the increased signaling endosomes and enhanced CAR-TRAF2 interaction could amplify 4-1BB signaling. Given that one of the major pathways activated by 4-1BB is the NF-κB pathway, we checked the phosphorylation of NF-κB and the expression level of antiapoptotic protein Bcl-xL and Bfl1, downstream targets of canonical NF-κB signal pathway (Lee et al., 2002; Wortzman et al., 2013). Indeed, 19BBζ^{KR} CAR-T cells showed increased phosphorylation level of NF-κB and enhanced transcriptional level of Bcl-xL and Bfl1 6–24 h after activation (Figures 5E and S6B). Furthermore, since there are several studies suggesting that mTOR activities are also associated with 4-1BB signaling (Kim et al., 2009; Teijeira

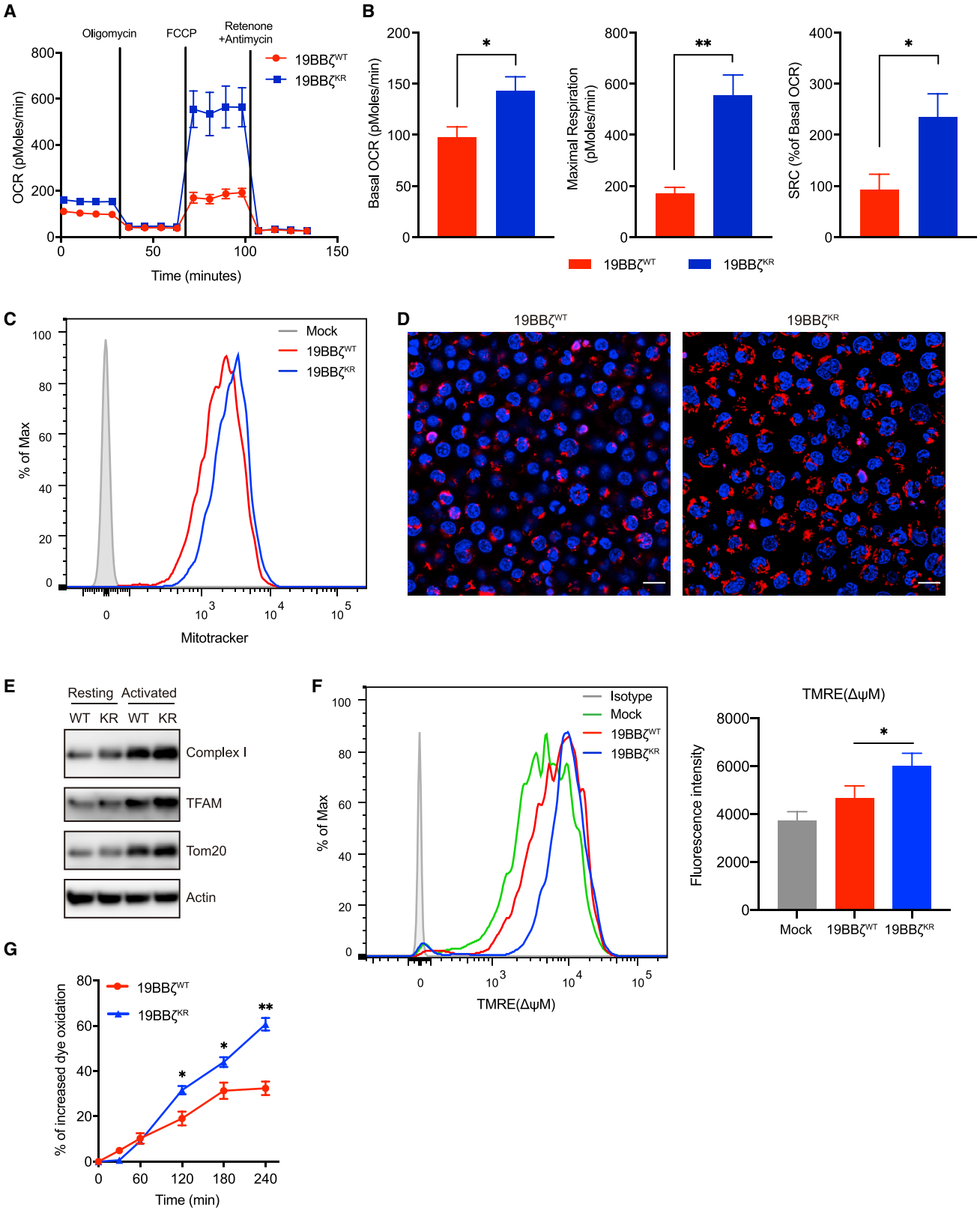

(legend on next page)

et al., 2018), we compared mTOR activities in CAR^{WT}-T and CAR^{KR}-T cells. Phosphorylation levels of two mTOR substrates, S6 and 4E-BP1, were quantitated by intracellular fluorescence-activated cell sorting (FACS) staining as indicators of mTOR activities (Figure S6C). We found that, like NF-κB signaling pathway, mTOR activities were also enhanced in CAR^{KR}-T cells compared with CAR^{WT}-T cells. In contrast, both CAR^{WT}-T cells and CAR^{KR}-T cells upregulated similar level of CD69, an activation marker induced by CD3ζ-ITAM signaling, following tumor antigen stimulation (Figure S6D), suggesting that the signaling amplification effect in CAR^{KR}-T cells is more limited to the signals downstream of 4-1BB. Similarly, endosomal signaling is reported to be only associated with 4-1BB signaling, but not other costimulatory motifs (e.g., CD28), the CARs containing other costimulatory domain may not benefit from the increase of endosomal CAR. To test this possibility, we examined the differentiation characteristics of *in vitro*-expanded CAR^{WT}-T and CAR^{KR}-T cells in the setting of second-generation CAR containing the CD28 costimulation domain. Indeed, compared to 1928ζ CAR^{WT}-T cells, 1928ζ CAR^{KR}-T cells showed no evidence of promoting Tcm cell formation in neither CD4 nor CD8 T cell subsets (Figure S6E). These data demonstrate that CAR^{KR} do not promote the memory T cell differentiation of CAR-T cells containing CD28 costimulation domain.

Overall, our data support the notion that blocking ubiquitination of CAR containing 4-1BB costimulation domain increases CAR-TRAF2 containing signaling endosomes and sustains 4-1BB-induced NF-κB and mTOR signaling.

19BBζ CAR^{KR}-T Cells Show Enhanced Mitochondrial Oxidative Phosphorylation and Biogenesis

Cellular metabolism has been appreciated to play a key role in regulating T cell differentiation and effector function after T cell activation (MacIver et al., 2013; Pearce and Pearce, 2013; Wang and Green, 2012). Enhanced mitochondrial fatty acid oxidation (FAO) promoted CD8+ memory T cell development after infection (Pearce et al., 2009; van der Windt et al., 2012). Moreover, it is reported that the 4-1BB signaling augments oxidative phosphorylation (OXPHOS), which promotes Tcm cell differentiation in CAR-T cells (Kawalekar et al., 2016). To compare the metabolism of CAR^{WT}-T and CAR^{KR}-T cells, we measured the oxygen consumption rate (OCR). 19BBζ CAR-T cells were examined after stimulation with irradiated target cells for 14 days. We found CAR^{KR}-T cells possessed significantly higher basal and maximal OCR than CAR^{WT}-T cells, suggesting a bias toward OXPHOS (Figures 6A and 6B). Sufficient mitochondrial spare respiratory capacity (SRC) is critical for stable memory T cell formation by providing energy under stressed conditions (Nicholls, 2009; Yadava and Nicholls, 2007). We consistently observed that CAR^{KR}-T cells generated a higher SRC level than CAR^{WT}-T cells (Figure 6B). We also observed that ECAR, an indicator of glycolysis, was also moderately increased in 19BBζ CAR^{KR}-T cells, which is consistent with previous study showing that 4-1BB signaling can activate both glucose and fatty acid metabolism in T cells (Choi et al., 2017). Yet, the fold of increased SRC is much higher than the fold of ECAR upregulation in CAR^{KR}-T cells (Figure S6F), suggesting a bias toward OXPHOS in CAR^{KR}-T cells. These results are consistent with the metabolic characteristics of long-lived memory T cells, which suggests that CAR^{KR} promotes Tcm cell differentiation of CAR-T cells incorporating 4-1BB costimulation domain via augmented OXPHOS flux.

Since the SRC is dependent on mitochondrial FAO, which positively correlates with mitochondrial mass (van der Windt et al., 2012), we checked whether 19BBζ CAR^{KR}-T cells maintain more mitochondrial mass. By performing both flow cytometry analysis and confocal microscopy imaging using MitoTracker staining, we found an increased mitochondrial mass of CAR^{KR}-T cells compared with CAR^{WT}-T cells (Figures 6C,6D, and S6G). Furthermore, we observed that mitochondria in 19BBζ CAR^{KR}-T cells were maintained as a fused network (Figure S6G), a metabolic hallmark of memory T cells (Buck et al., 2016). These results support our finding that 19BBζ CAR^{KR}-T cells promoted memory cell formation. In accordance with the increased mitochondrial content, we found that activated CAR^{KR}-T cells generated more mRNA of MT-CO1, which is encoded by the mitochondrial genome, and TFAM, a mitochondrial gene encoded by the nuclear genome, than CAR^{WT}-T cells (Figure S6H). NRF1 and NRF2, two mitochondrial-function-associated transcription factors, also showed significantly increased expression in stimulated CAR^{KR}-T cells, which strongly support its enhanced OXPHOS flux (Figure S6H). We also found that the protein expression levels of TFAM, NDUFB8 (a subunit of complex I), and the mitochondrial import receptor Tom20 were increased in activated CAR^{KR}-T cells compared to activated CAR^{WT}-T cells (Figure 6E). In addition, we measured mitochondrial membrane potential (Figure 6F) and ROS induction upon CAR-T activation (Figure 6G). Our results revealed that CAR^{KR}-T cells had higher mitochondrial membrane potential and generated more activation-induced ROS than CAR^{WT}-T cells. Together, these results demonstrate that 19BBζ CAR^{KR}-T cells exhibited enhanced mitochondrial biogenesis and function, which contribute to their promoted memory T cell differentiation and prolonged T cell persistence.

DISCUSSION

CAR-T therapy is a promising approach in cancer immunotherapy, but it may be limited by the poor *in vivo* expansion and persistence of CAR-T cells after infusion. Herein, we investigated whether

Figure 6. 19BBζ CAR^{KR}-T Cells Show Enhanced Mitochondrial Oxidative Phosphorylation and Biogenesis

(A) The oxygen consumption rates (OCRs) of CAR-T cells after stimulation of irradiated target cells.

(B) Basal OCR levels, maximum respiratory levels, and spare respiratory capacity (SRC) measured 14 days after stimulation with irradiated target cells.

(C) FACS analysis of mitochondrial mass in the CAR-T cells by using MitoTracker.

(D) Confocal image of CAR-T cells stained with Hoechst (blue) and MitoTracker (red). Scale bars,10 μm. See also Figure S6.

(E) Western blot analysis of mitochondrial associated proteins in the CAR-T cells.

(F) Mitochondrial membrane potential analysis of CAR-T cells. Representative of four donors.

(G) ROS level in CAR-T cells stimulated with target cells for indicated time.

All data acquired from at least three independent experiments and represented as mean ± SEM (*$p < 0.05$, **$p < 0.01$).

CAR-T cell persistence and functionality could be optimized by redirecting the trafficking of CAR molecules. We reveal that tumor antigen triggers rapid ubiquitination of the CAR, which targets internalization of the CAR for lysosomal degradation and results in CAR downmodulation. Blocking CAR ubiquitination via substitution of all cytoplasmic lysines with arginines resulted in inhibiting lysosomal degradation of CAR, which led to inefficient CAR downmodulation. Therefore, we named this type of CAR as a recyclable CAR. Recyclable CAR has two important features. First, the downmodulation of the recyclable CAR following ligation of tumor antigens is significantly inhibited, which likely leads to more effective long-term tumor killing. Second, recyclable BBζ CAR-T cells contain more signaling endosomes that amplify 4-1BB signal transduction and facilitate the metabolic reprograming of the CAR-T cells toward oxidative phosphorylation. Therefore, recyclable BBζ CAR-T cells show enhanced memory T cell development and improved *in vivo* persistence. Overall, our study has demonstrated that the recyclable CAR-T cells have a superior antitumor activity, which may offer a straightforward and universal solution to enhancing persistence and functionality of CAR-T cells containing 4-1BB signaling domains.

Following ligand encounter, receptors initiate the signal transduction at the cell surface. However, it has been demonstrated that a number of receptors such as EGFR, NGF, and 4-1BB are able to signal via their endosomal pools inside of the cell (Bakker et al., 2017; Howe et al., 2001; Martinez-Forero et al., 2013). 4-1BB is a costimulatory receptor on T lymphocytes (Kwon and Weissman, 1989) and stimulation of 4-1BB receptor with agonist antibody elicits a potent antitumor function *in vivo* (Halstead et al., 2002). Interestingly, it has been demonstrated that 4-1BB agonist monoclonal antibodies (mAbs) trigger 4-1BB internalization to an endosomal compartment and endocytosed 4-1BB-containing vesicles recruit TRAF2, which form an active signaling complex to further activate downstream signaling. Whereas it is appreciated that multiple receptor systems use "signaling endosomes," it is not clear whether signaling endosomes participate in CAR-T signaling. Here, we show that, after engagement of tumor antigen, the second-generation CAR containing 4-1BB costimulatory domain is internalized to early endosomes. Importantly, our results suggest that these CAR endosomes might function as an active signaling complex in T cells. First, TRAF2, a crucial player of 4-1BB signaling, is recruited to these BBζ CAR containing endosomes in a 4-1BB domain-dependent manner. Second, our study demonstrated that the turnover of CAR signaling endosomes is controlled by CAR ubiquitination. Blocking CAR ubiquitination significantly increased the number of signaling endosomes. We also showed that the number of signaling endosomes containing 19BBζ CAR positively correlates with the strength of 4-1BB downstream signaling. Collectively, these results suggest that 19BBζ CAR signaling can be propagated in endosomes. How 4-1BB CAR signaling endosome function is regulated is an interesting question for future investigation, which may help optimize CAR-T function.

In contrast to amplification of 4-1BB signaling, the signaling events downstream of CD3ζ-ITAM, such as the recruitment of ZAP-70 to CARs, phosphorylation of LAT, and upregulation of CD69, are largely not altered in CAR^{KR}-T cells. Why does the recyclable CAR design selectively enhance 4-1BB signaling activities, but not CD3ζ-ITAM signaling? There are at least two possibilities. First, it may be because the signaling endosome is a unique feature of 4-1BB signaling. The internalized 4-1BB containing early endosomes remain as an active signaling complex that actively recruit the effector TRAF2 proteins (Martinez-Forero et al., 2013; Zapata et al., 2018). Yet, there is no evidence that endosomal CD3ζ-ITAM could efficiently recruit its effector protein ZAP-70. The recruitment of ZAP-70 to CD3-ITAM is essential for TCR signal transduction and therefore is tightly regulated, e.g., requiring Lck that phosphorylates ZAP-70 to stabilize the interaction between ZAP-70 and ITAM (Klammt et al., 2015). Upon T cell activation, surface TCR is rapidly downmodulated, but Lck proteins are strictly retained at the cell surface in activated T cells (Compeer et al., 2018). Thus, we speculated that the endosomal CD3ζ-ITAM may not efficiently recruit its effector protein ZAP-70 due to a lack of Lck proteins in these internalized endosomes. Second, it is recently reported that the 4-1BB domain of BBζ CAR can actively recruit THEMIS-SHP1 complex, in which the phosphatase SHP1 counteracts the effect of LCK, a proximal kinase of TCR signaling (Sun et al., 2020; Wang et al., 2010b). We indeed observed that, upon CAR-T activation, more THEMIS proteins were recruited to CAR^{KR} than CAR^{WT}. Therefore, it is possible that, although the blocking CAR ubiquitination may sustain CAR signaling in general, the 4-1BB-associated THEMIS-SHP1 complex acts as a safety check to prevent overactivation of CD3ζ-ITAM signaling.

In addition to observing inefficient downmodulation and increased endosomal CAR^{KR} level after CAR-T activation, counterintuitively, we also saw a reduction of surface CAR expression in the resting CAR^{KR}-T cells compared with CAR^{WT}-T cells. Interestingly, similar observations were also reported in the case of TCR. When ubiquitination of TCR:CD3 complex was blocked by mutating all intracellular lysines of CD3 chains to arginines, the surface TCR expression on resting mature T cells has an approximately 40% reduction compared to wild-type TCR (Wang et al., 2010a). Moreover, deficiency of Cbl, a major E3 ligase of the TCR:CD3 complex, or a loss-of-function mutant of Cbl also results in a similar reduction of surface TCR expression on resting mature T cells (Thien et al., 2003). Consistent with the comparable mRNA levels of CAR^{WT} and CAR^{KR}, both CARs were expressed at similar protein amounts. Considering the reduced surface CAR level on CAR^{KR}-T cells, we conclude that there is more cytosolic fraction of CAR^{KR} than that of CAR^{WT}. These results suggested that newly synthesized CAR^{KR} may not traffic to the cell membrane as efficiently as CAR^{WT}. Since we have observed a constitutive but low ubiquitination of CAR in resting CAR-T cells, it is intuitive to speculate that basal CAR ubiquitination in resting T cells is involved in regulating the transport of CAR to the plasma membrane. Alternatively, this phenotype may be caused by increased CAR signaling strength due to enhanced CAR endosomal signaling, which may induce an unknown feedback mechanism to repress the surface CAR expression. The underlying mechanism(s) by which CAR^{KR} displayed a lower CAR surface expression are currently under investigation.

Previous studies suggested that CAR expression positively correlates with tonic signaling, which can induce T cell exhaustion and limit the potency of CAR T cells (Long et al., 2015). Is it possible that superior antitumor efficacy of the BBζ CAR^{KR}-T cells simply results from its lower surface expression? In another words, does lower surface expression of BBζ CAR lead into better

antitumor function *in vivo*? A recent study addressed this question by replacing the EF-1α promoter of BBζ CAR, with a truncated promoter from the Phosphoglycerate kinase (PGK) promoter. Although displaying 50%–60% lower cell-surface CAR expression levels than wild-type BBζ CAR-T cells, these modified CAR-T cells significantly diminished their antitumor function in a xenograft pancreatic tumor model (Guedan et al., 2018). Similarly, Walker et al. tuned CAR expression level by using titrated retrovirus at different multiplicities of infection. In setting of ALK-BBζ CAR and 19BBζ CAR, downstream NFAT activation and cytokine production of low CAR-expressing cells was largely impaired compared to high CAR-expressing cells (Walker et al., 2017). Importantly, we also demonstrated that the better tumor-killing capacity of CAR^{KR}-T cells is not due to the reduction of its initial surface CAR expression level on resting CAR-T cells. These results suggest that lower BBζ CAR expression is not generally beneficial, and therefore, the superior antitumor efficacy BBζ CAR^{KR} is unlikely caused by its lower surface expression.

The *in vitro*-transcribed (IVT) mRNA approach is frequently used for the development, testing, and application of CAR-T therapy (Foster et al., 2019). Because of its inherent safety, several clinical trials of mRNA CAR-T are ongoing. However, rapid loss of expression of CAR is the major obstacle to limit its efficacy. Here, we show that recyclable CAR dramatically prolonged half-life of CAR protein following tumor antigen stimulation compared with CAR^{WT}, which may offer a potential solution to optimize pharmacokinetic properties of RNA CAR.

In summary, we demonstrate that, as many other immune receptors, synthetic CAR surface expression is also dynamically regulated during the CAR-T activation. Our study suggests that manipulation of CAR trafficking within T cells is a useful strategy to optimize CAR-T antitumor function. Overall, our study suggests that the recyclable CAR-T cells have better long-term killing, improved persistence, and augmented antitumor function, which provides a solid rationale to test recyclable CAR-T cells in human trials.

Limitations of the Study

Here, we showed that the recyclable CAR-T cells displayed enhanced *in vivo* persistence using CAR-T cells that are generated by lentiviral transduction. It needs to be further tested whether the recyclable CAR design would benefit the CAR-T cells that are produced by other methods (e.g., retroviral transduction or IVT). This study also used an immunocompromised mouse model with xenografted human tumor cell line, which can't fully mimic the complex immune environment within cancer patients. The optimal antitumor benefit of recyclable CAR needs to be further tested in clinical trials.

STAR★METHODS

Detailed methods are provided in the online version of this paper and include the following:

SUPPLEMENTAL INFORMATION

Supplemental Information can be found online at https://doi.org/10.1016/j.immuni.2020.07.011.

ACKNOWLEDGMENTS

We are grateful for advice from A. Weiss (UCSF), T. Chi, Z. Lin (ShanghaiTech), and B.B. Au-Yeung (Emory). We thank the staff members of the Animal Facility at the National Facility for Protein Science in Shanghai, Zhangjiang Lab for providing the support in mouse housing and care, and the staff members of the FACS, Mass Spectrometry and Image Facility of ShanghaiTech for technical supports. This work was supported by 2019YFA0111000 from National Key R&D Program of China, China (H. Wang); 31670919 (H. Wang), 31530022 (C.X.), 31861133009 (C.X.), and 31621003 (C.X.) from National Natural Science Foundation of China, China; 17411962000 from Science and Technology Commission of Shanghai Municipality of China, China (H. Wu); 2019SY059 from Health and Family Planning Commission of Shanghai Municipality of China, China (H. Wu). C.X. is also funded by XDB29000000, QYZDB-SSW-SMC048, and Fountain-Valley Life Sciences Fund from Chinese Academy of Sciences, China.

AUTHOR CONTRIBUTIONS

H. Wang, C.X., and H. Wu designed the experiments and wrote the manuscript. W.L., S.Q., and J.C. performed and analyzed the experiments. S.J., W.C., J.J., F.W., W.S., Y.S. P.W., G.F., and R.T. provided resources and performed and analyzed specific experiments.

DECLARATION OF INTERESTS

A patent application has been submitted based on results presented in this manuscript. H. Wang, P.W., W.L., and S.Q. are listed as the inventors. The authors declare no competing interests.

Received: January 7, 2020
Revised: April 21, 2020
Accepted: July 15, 2020
Published: August 5, 2020

REFERENCES

Acconcia, F., Sigismund, S., and Polo, S. (2009). Ubiquitin in trafficking: the network at work. Exp. Cell Res. *315*, 1610–1618.

Ahmed, N., Brawley, V.S., Hegde, M., Robertson, C., Ghazi, A., Gerken, C., Liu, E., Dakhova, O., Ashoori, A., Corder, A., et al. (2015). Human Epidermal Growth Factor Receptor 2 (HER2) -Specific Chimeric Antigen Receptor-Modified T Cells for the Immunotherapy of HER2-Positive Sarcoma. J. Clin. Oncol. *33*, 1688–1696.

Bakker, J., Spits, M., Neefjes, J., and Berlin, I. (2017). The EGFR odyssey - from activation to destruction in space and time. J. Cell Sci. *130*, 4087–4096.

Berger, C., Jensen, M.C., Lansdorp, P.M., Gough, M., Elliott, C., and Riddell, S.R. (2008). Adoptive transfer of effector CD8+ T cells derived from central memory cells establishes persistent T cell memory in primates. J. Clin. Invest. *118*, 294–305.

Buck, M.D., O'Sullivan, D., Klein Geltink, R.I., Curtis, J.D., Chang, C.H., Sanin, D.E., Qiu, J., Kretz, O., Braas, D., van der Windt, G.J., et al. (2016). Mitochondrial Dynamics Controls T Cell Fate through Metabolic Programming. Cell *166*, 63–76.

Caruso, H.G., Hurton, L.V., Najjar, A., Rushworth, D., Ang, S., Olivares, S., Mi, T., Switzer, K., Singh, H., Huls, H., et al. (2015). Tuning Sensitivity of CAR to EGFR Density Limits Recognition of Normal Tissue While Maintaining Potent Antitumor Activity. Cancer Res. *75*, 3505–3518.

Choi, B.K., Lee, D.Y., Lee, D.G., Kim, Y.H., Kim, S.H., Oh, H.S., Han, C., and Kwon, B.S. (2017). 4-1BB signaling activates glucose and fatty acid metabolism to enhance $CD8^+$ T cell proliferation. Cell. Mol. Immunol. *14*, 748–757.

Compeer, E.B., Kraus, F., Ecker, M., Redpath, G., Amiezer, M., Rother, N., Nicovich, P.R., Kapoor-Kaushik, N., Deng, Q., Samson, G.P.B., et al. (2018). A mobile endocytic network connects clathrin-independent receptor endocytosis to recycling and promotes T cell activation. Nat. Commun. *9*, 1597.

Davenport, A.J., Jenkins, M.R., Cross, R.S., Yong, C.S., Prince, H.M., Ritchie, D.S., Trapani, J.A., Kershaw, M.H., Darcy, P.K., and Neeson, P.J. (2015). CAR-T Cells Inflict Sequential Killing of Multiple Tumor Target Cells. Cancer Immunol. Res. *3*, 483–494.

Eyquem, J., Mansilla-Soto, J., Giavridis, T., van der Stegen, S.J., Hamieh, M., Cunanan, K.M., Odak, A., Gönen, M., and Sadelain, M. (2017). Targeting a CAR to the TRAC locus with CRISPR/Cas9 enhances tumour rejection. Nature *543*, 113–117.

Foster, J.B., Barrett, D.M., and Kariko, K. (2019). The Emerging Role of In Vitro-Transcribed mRNA in Adoptive T Cell Immunotherapy. Mol Ther. *27*, 747–756.

Fraietta, J.A., Nobles, C.L., Sammons, M.A., Lundh, S., Carty, S.A., Reich, T.J., Cogdill, A.P., Morrissette, J.J.D., DeNizio, J.E., Reddy, S., et al. (2018). Disruption of TET2 promotes the therapeutic efficacy of CD19-targeted T cells. Nature *558*, 307–312.

Gattinoni, L., Lugli, E., Ji, Y., Pos, Z., Paulos, C.M., Quigley, M.F., Almeida, J.R., Gostick, E., Yu, Z., Carpenito, C., et al. (2011). A human memory T cell subset with stem cell-like properties. Nat. Med. *17*, 1290–1297.

Guedan, S., Posey, A.D., Jr., Shaw, C., Wing, A., Da, T., Patel, P.R., McGettigan, S.E., Casado-Medrano, V., Kawalekar, O.U., Uribe-Herranz, M., et al. (2018). Enhancing CAR T cell persistence through ICOS and 4-1BB costimulation. JCI Insight *3*, e96976.

Haglund, K., and Dikic, I. (2005). Ubiquitylation and cell signaling. EMBO J. *24*, 3353–3359.

Halstead, E.S., Mueller, Y.M., Altman, J.D., and Katsikis, P.D. (2002). In vivo stimulation of CD137 broadens primary antiviral CD8+ T cell responses. Nat. Immunol. *3*, 536–541.

Hamieh, M., Dobrin, A., Cabriolu, A., van der Stegen, S.J.C., Giavridis, T., Mansilla-Soto, J., Eyquem, J., Zhao, Z., Whitlock, B.M., Miele, M.M., et al. (2019). CAR T cell trogocytosis and cooperative killing regulate tumour antigen escape. Nature *568*, 112–116.

Hicke, L., and Dunn, R. (2003). Regulation of membrane protein transport by ubiquitin and ubiquitin-binding proteins. Annu. Rev. Cell Dev. Biol. *19*, 141–172.

Hicke, L., and Riezman, H. (1996). Ubiquitination of a yeast plasma membrane receptor signals its ligand-stimulated endocytosis. Cell *84*, 277–287.

Howe, C.L., Valletta, J.S., Rusnak, A.S., and Mobley, W.C. (2001). NGF signaling from clathrin-coated vesicles: evidence that signaling endosomes serve as a platform for the Ras-MAPK pathway. Neuron *32*, 801–814.

Jensen, M.C., Popplewell, L., Cooper, L.J., DiGiusto, D., Kalos, M., Ostberg, J.R., and Forman, S.J. (2010). Antitransgene rejection responses contribute to attenuated persistence of adoptively transferred CD20/CD19-specific chimeric antigen receptor redirected T cells in humans. Biol. Blood Marrow Transplant. *16*, 1245–1256.

Kawalekar, O.U., O'Connor, R.S., Fraietta, J.A., Guo, L., McGettigan, S.E., Posey, A.D., Jr., Patel, P.R., Guedan, S., Scholler, J., Keith, B., et al. (2016). Distinct Signaling of Coreceptors Regulates Specific Metabolism Pathways and Impacts Memory Development in CAR T Cells. Immunity *44*, 380–390.

Kershaw, M.H., Westwood, J.A., Parker, L.L., Wang, G., Eshhar, Z., Mavroukakis, S.A., White, D.E., Wunderlich, J.R., Canevari, S., Rogers-Freezer, L., et al. (2006). A phase I study on adoptive immunotherapy using gene-modified T cells for ovarian cancer. Clin. Cancer Res. *12*, 6106–6115.

Kim, D.K., Lee, S.C., and Lee, H.W. (2009). CD137 ligand-mediated reverse signals increase cell viability and cytokine expression in murine myeloid cells: involvement of mTOR/p70S6 kinase and Akt. Eur. J. Immunol. *39*, 2617–2628.

Klammt, C., Novotná, L., Li, D.T., Wolf, M., Blount, A., Zhang, K., Fitchett, J.R., and Lillemeier, B.F. (2015). T cell receptor dwell times control the kinase activity of Zap70. Nat. Immunol. *16*, 961–969.

Kwon, B.S., and Weissman, S.M. (1989). cDNA sequences of two inducible T-cell genes. Proc. Natl. Acad. Sci. USA *86*, 1963–1967.

Lamers, C.H.J., Gratama, J.W., Pouw, N.M.C., Langeveld, S.C.L., Krimpen, B.A., Kraan, J., Stoter, G., and Debets, R. (2005). Parallel detection of transduced T lymphocytes after immunogene therapy of renal cell cancer by flow cytometry and real-time polymerase chain reaction: implications for loss of transgene expression. Hum. Gene Ther. *16*, 1452–1462.

Lamers, C.H., Sleijfer, S., Vulto, A.G., Kruit, W.H., Kliffen, M., Debets, R., Gratama, J.W., Stoter, G., and Oosterwijk, E. (2006). Treatment of metastatic renal cell carcinoma with autologous T-lymphocytes genetically retargeted against carbonic anhydrase IX: first clinical experience. J. Clin. Oncol. *24*, e20–e22.

Lee, H.W., Park, S.J., Choi, B.K., Kim, H.H., Nam, K.O., and Kwon, B.S. (2002). 4-1BB promotes the survival of CD8+ T lymphocytes by increasing expression of Bcl-xL and Bfl-1. J. Immunol. *169*, 4882–4888.

Li, G., Boucher, J.C., Kotani, H., Park, K., Zhang, Y., Shrestha, B., Wang, X., Guan, L., Beatty, N., Abate-Daga, D., and Davila, M.L. (2018). 4-1BB enhancement of CAR T function requires NF-κB and TRAFs. JCI Insight *3*, e121322.

Liu, H., Rhodes, M., Wiest, D.L., and Vignali, D.A. (2000). On the dynamics of TCR:CD3 complex cell surface expression and downmodulation. Immunity *13*, 665–675.

Long, A.H., Haso, W.M., Shern, J.F., Wanhainen, K.M., Murgai, M., Ingaramo, M., Smith, J.P., Walker, A.J., Kohler, M.E., Venkateshwara, V.R., et al. (2015). 4-1BB costimulation ameliorates T cell exhaustion induced by tonic signaling of chimeric antigen receptors. Nat. Med. *21*, 581–590.

MacIver, N.J., Michalek, R.D., and Rathmell, J.C. (2013). Metabolic regulation of T lymphocytes. Annu. Rev. Immunol. *31*, 259–283.

Martinez-Forero, I., Azpilikueta, A., Bolaños-Mateo, E., Nistal-Villan, E., Palazon, A., Teijeira, A., Perez-Chacon, G., Morales-Kastresana, A., Murillo, O., Jure-Kunkel, M., et al. (2013). T cell costimulation with anti-CD137 monoclonal antibodies is mediated by K63-polyubiquitin-dependent signals from endosomes. J. Immunol. *190*, 6694–6706.

Maude, S.L., Frey, N., Shaw, P.A., Aplenc, R., Barrett, D.M., Bunin, N.J., Chew, A., Gonzalez, V.E., Zheng, Z., Lacey, S.F., et al. (2014). Chimeric antigen receptor T cells for sustained remissions in leukemia. N. Engl. J. Med. *371*, 1507–1517.

Maude, S.L., Laetsch, T.W., Buechner, J., Rives, S., Boyer, M., Bittencourt, H., Bader, P., Verneris, M.R., Stefanski, H.E., Myers, G.D., and Qayed, M. (2018). Tisagenlecleucel in Children and Young Adults with B-Cell Lymphoblastic Leukemia. N. Engl. J. Med. *378*, 439–448.

Menk, A.V., Scharping, N.E., Rivadeneira, D.B., Calderon, M.J., Watson, M.J., Dunstane, D., Watkins, S.C., and Delgoffe, G.M. (2018). 4-1BB costimulation induces T cell mitochondrial function and biogenesis enabling cancer immunotherapeutic responses. J. Exp. Med. *215*, 1091–1100.

Naramura, M., Jang, I.K., Kole, H., Huang, F., Haines, D., and Gu, H. (2002). c-Cbl and Cbl-b regulate T cell responsiveness by promoting ligand-induced TCR down-modulation. Nat. Immunol. *3*, 1192–1199.

Neelapu, S.S., Locke, F.L., Bartlett, N.L., Lekakis, L.J., Miklos, D.B., Jacobson, C.A., Braunschweig, I., Oluwole, O.O., Siddiqi, T., Lin, Y., et al. (2017). Axicabtagene Ciloleucel CAR T-Cell Therapy in Refractory Large B-Cell Lymphoma. N. Engl. J. Med. *377*, 2531–2544.

Nicholls, D.G. (2009). Spare respiratory capacity, oxidative stress and excitotoxicity. Biochem. Soc. Trans. *37*, 1385–1388.

Nicholson, I.C., Lenton, K.A., Little, D.J., Decorso, T., Lee, F.T., Scott, A.M., Zola, H., and Hohmann, A.W. (1997). Construction and characterisation of a functional CD19 specific single chain Fv fragment for immunotherapy of B lineage leukaemia and lymphoma. Mol. Immunol. *34*, 1157–1165.

Park, J.H., Rivière, I., Gonen, M., Wang, X., Sénéchal, B., Curran, K.J., Sauter, C., Wang, Y., Santomasso, B., Mead, E., et al. (2018). Long-Term Follow-up of CD19 CAR Therapy in Acute Lymphoblastic Leukemia. N. Engl. J. Med. *378*, 449–459.

Pearce, E.L., and Pearce, E.J. (2013). Metabolic pathways in immune cell activation and quiescence. Immunity *38*, 633–643.

Pearce, E.L., Walsh, M.C., Cejas, P.J., Harms, G.M., Shen, H., Wang, L.S., Jones, R.G., and Choi, Y. (2009). Enhancing CD8 T-cell memory by modulating fatty acid metabolism. Nature *460*, 103–107.

Porter, D.L., Hwang, W.T., Frey, N.V., Lacey, S.F., Shaw, P.A., Loren, A.W., Bagg, A., Marcucci, K.T., Shen, A., Gonzalez, V., et al. (2015). Chimeric antigen receptor T cells persist and induce sustained remissions in relapsed refractory chronic lymphocytic leukemia. Sci. Transl. Med. *7*, 303ra139.

Radvanyi, L.G., Bernatchez, C., Zhang, M., Fox, P.S., Miller, P., Chacon, J., Wu, R., Lizee, G., Mahoney, S., Alvarado, G., et al. (2012). Specific lymphocyte subsets predict response to adoptive cell therapy using expanded autologous tumor-infiltrating lymphocytes in metastatic melanoma patients. Clin Cancer Res. *18*, 6758–6770.

Rossig, C., Bollard, C.M., Nuchtern, J.G., Merchant, D.A., and Brenner, M.K. (2001). Targeting of G(D2)-positive tumor cells by human T lymphocytes engineered to express chimeric T-cell receptor genes. Int. J. Cancer *94*, 228–236.

Saoulli, K., Lee, S.Y., Cannons, J.L., Yeh, W.C., Santana, A., Goldstein, M.D., Bangia, N., DeBenedette, M.A., Mak, T.W., Choi, Y., and Watts, T.H. (1998). CD28-independent, TRAF2-dependent costimulation of resting T cells by 4-1BB ligand. J. Exp. Med. *187*, 1849–1862.

Schmidts, A., and Maus, M.V. (2018). Making CAR T Cells a Solid Option for Solid Tumors. Front. Immunol. *9*, 2593.

Schuster, S.J., Svoboda, J., Chong, E.A., Nasta, S.D., Mato, A.R., Anak, Ö., Brogdon, J.L., Pruteanu-Malinici, I., Bhoj, V., Landsburg, D., et al. (2017). Chimeric Antigen Receptor T Cells in Refractory B-Cell Lymphomas. N. Engl. J. Med. *377*, 2545–2554.

Sun, C., Shou, P., Du, H., Hirabayashi, K., Chen, Y., Herring, L.E., Ahn, S., Xu, Y., Suzuki, K., Li, G., et al. (2020). THEMIS-SHP1 Recruitment by 4-1BB Tunes LCK-Mediated Priming of Chimeric Antigen Receptor-Redirected T Cells. Cancer Cell *37*, 216–225.e6.

Teijeira, A., Labiano, S., Garasa, S., Etxeberria, I., Santamaría, E., Rouzaut, A., Enamorado, M., Azpilikueta, A., Inoges, S., Bolaños, E., et al. (2018). Mitochondrial Morphological and Functional Reprogramming Following CD137 (4-1BB) Costimulation. Cancer Immunol. Res. *6*, 798–811.

Thien, C.B.F., Scaife, R.M., Papadimitriou, J.M., Murphy, M.A., Bowtell, D.D.L., and Langdon, W.Y. (2003). A mouse with a loss-of-function mutation in the c-Cbl TKB domain shows perturbed thymocyte signaling without enhancing the activity of the ZAP-70 tyrosine kinase. J. Exp. Med. *197*, 503–513.

van der Windt, G.J.W., Everts, B., Chang, C.H., Curtis, J.D., Freitas, T.C., Amiel, E., Pearce, E.J., and Pearce, E.L. (2012). Mitochondrial respiratory capacity is a critical regulator of CD8+ T cell memory development. Immunity *36*, 68–78.

Walker, A.J., Majzner, R.G., Zhang, L., Wanhainen, K., Long, A.H., Nguyen, S.M., Lopomo, P., Vigny, M., Fry, T.J., Orentas, R.J., and Mackall, C.L. (2017). Tumor Antigen and Receptor Densities Regulate Efficacy of a Chimeric Antigen Receptor Targeting Anaplastic Lymphoma Kinase. Mol Ther. *25*, 2189–2201.

Wang, R., and Green, D.R. (2012). Metabolic checkpoints in activated T cells. Nat. Immunol. *13*, 907–915.

Wang, H., Holst, J., Woo, S.R., Guy, C., Bettini, M., Wang, Y., Shafer, A., Naramura, M., Mingueneau, M., Dragone, L.L., et al. (2010a). Tonic ubiquitylation controls T-cell receptor:CD3 complex expression during T-cell development. EMBO J. *29*, 1285–1298.

Wang, H., Kadlecek, T.A., Au-Yeung, B.B., Goodfellow, H.E., Hsu, L.Y., Freedman, T.S., and Weiss, A. (2010b). ZAP-70: an essential kinase in T-cell signaling. Cold Spring Harb. Perspect. Biol. *2*, a002279.

Watanabe, K., Kuramitsu, S., Posey, A.D., Jr., and June, C.H. (2018). Expanding the Therapeutic Window for CAR T Cell Therapy in Solid Tumors: The Knowns and Unknowns of CAR T Cell Biology. Front. Immunol. *9*, 2486.

Watts, T.H., Lin, G.H., Wang, C., McPherson, A.J., Snell, L.M., and Sabbagh, L. (2011). Role of 4-1BBL and TRAF1 in the CD8 T cell response to influenza virus and HIV. Adv. Exp. Med. Biol. *691*, 177–186.

Wortzman, M.E., Clouthier, D.L., McPherson, A.J., Lin, G.H., and Watts, T.H. (2013). The contextual role of TNFR family members in CD8(+) T-cell control of viral infections. Immunol. Rev. *255*, 125–148.

Yadava, N., and Nicholls, D.G. (2007). Spare respiratory capacity rather than oxidative stress regulates glutamate excitotoxicity after partial respiratory inhibition of mitochondrial complex I with rotenone. J. Neurosci. *27*, 7310–7317.

Yang, C.W., Hojer, C.D., Zhou, M., Wu, X., Wuster, A., Lee, W.P., Yaspan, B.L., and Chan, A.C. (2016). Regulation of T Cell Receptor Signaling by DENND1B in TH2 Cells and Allergic Disease. Cell *164*, 141–155.

Zapata, J.M., Perez-Chacon, G., Carr-Baena, P., Martinez-Forero, I., Azpilikueta, A., Otano, I., and Melero, I. (2018). CD137 (4-1BB) Signalosome: Complexity Is a Matter of TRAFs. Front. Immunol. *9*, 2618.

Zhao, Z., Condomines, M., van der Stegen, S.J.C., Perna, F., Kloss, C.C., Gunset, G., Plotkin, J., and Sadelain, M. (2015). Structural Design of Engineered Costimulation Determines Tumor Rejection Kinetics and Persistence of CAR T Cells. Cancer Cell *28*, 415–428.

STAR★METHODS

KEY RESOURCES TABLE

REAGENT or RESOURCE	SOURCE	IDENTIFIER
Antibodies		
Anti-human CD3-PE/Cy7 (UCHT1)	eBioscience	Cat# 25-0038-42; RRID: AB_1582253
Anti-human CD3-APC (HIT3a)	Biolegend	Cat# 300412; RRID: AB_314066
Anti-human CD4-BV605 (RPA-T4)	Biolegend	Cat# 300556; RRID: AB_2564391
Anti-human CD8α-PerCP/Cy5.5 (RPA-T8)	Biolegend	Cat# 301032; RRID: AB_893422
Anti-human CD27-Alexa Fluor 647 (O323)	Biolegend	Cat# 302812; RRID: AB_493082
Anti-human CD45RA-PE/Cy7 (HI100)	Biolegend	Cat# 304125; RRID: AB_10709440
Anti-human CD45RO-PE/Cy7 (UCHL1)	Biolegend	Cat# 304230; RRID: AB_11203900
Anti-human CD62L-PE (DREG-56)	Biolegend	Cat# 304806; RRID: AB_314466
Anti-human CD69-PE (FN50)	Biolegend	Cat# 310906; RRID: AB_314841
Anti-human CD19-PE (HIB19)	Biolegend	Cat# 302254; RRID: AB_2564142
Anti-human PD-1-APC (NAT105)	Biolegend	Cat# 367405; RRID: AB_2566066
Anti-human PD-1-PE (eBioJ105)	eBioscience	Cat# 12-2799-42; RRID: AB_11042478
Anti-human LAG-3-PE/Cy7 (3DS233H)	eBioscience	Cat# 12-2239-42; RRID: AB_2572597
Anti-human Tim-3-PerCP/Cy5.5 (F38-2E2)	Biolegend	Cat# 345016; RRID: AB_2561934
Anti-human IL-2-PE (MQ1-17H12)	Biolegend	Cat# 500307; RRID: AB_315094
Anti-human IFN-γ-Alexa Fluor 647 (4S.B3)	Biolegend	Cat# 502516; RRID: AB_493031
Anti-human Granzyme B-Alexa Fluor 647 (GB11)	Biolegend	Cat# 515406; RRID: AB_2566333
Anti-human Ganglioside GD2-PE (14G2a)	Biolegend	Cat# 357303; RRID: AB_2561884
Anti-MYC-Alexa Fluor 647 (9B11)	Cell Signaling Technology	Cat# 2233; RRID: AB_823474
Anti-MYC-HRP (9B11)	Cell Signaling Technology	Cat# 2040; RRID: AB_2148465
Anti-NFkB pSer^{536} (93H1)	Cell Signaling Technology	Cat# 3033; RRID: AB_331284
Anti-S6 pSer$^{235/236}$ (D57.2.2E)	Cell Signaling Technology	Cat# 4858; RRID: AB_916156
Anti-4E-BP1 pThr$^{37/46}$ (236B4)	Cell Signaling Technology	Cat# 2855; RRID: AB_560835
Anti-LAT (E3U6J)	Cell Signaling Technology	Cat# 45533
Anti-LAT pY^{191}	Cell Signaling Technology	Cat# 3584; RRID: AB_2157728
Anti-p85 (19H8)	Cell Signaling Technology	Cat# 4257; RRID: AB_659889
Anti-TRAF2 (C192)	Cell Signaling Technology	Cat# 4724; RRID: AB_2209845
Anti-TFAM (D5C8)	Cell Signaling Technology	Cat# 8076; RRID: AB_10949110
Anti-ZAP70 (99F2)	Cell Signaling Technology	Cat# 2705; RRID: AB_2273231
Anti-α-tubulin (DM1A)	Abcam	Cat# ab40742; RRID: AB_880625
Anti-Rab5 (C8B1)	Cell Signaling Technology	Cat# 3547; RRID: AB_2300649
Anti-THEMIS	Cell Signaling Technology	Cat# 4482; RRID: AB_11217437
Anti-Tom20 (F-10)	Santa Cruz	Cat# sc-17764; RRID: AB_628381
Anti-GFP (7G9)	Abmart	Cat# M20004; RRID: AB_2619674
Anti-NDUFB8 (20E9DH10C12)	Abcam	Cat# ab110242; RRID: AB_10859122
Anti-GAPDH-HRP (6C5)	Abcam	Cat# ab105428; RRID: AB_10860607
Anti-Ubiquitin-HRP (P4D1)	Biolegend	Cat# 646303; RRID: AB_2629597
Anti-p62 (3/P62 LCK LIGAND)	BD Bioscience	Cat# 610832; RRID: AB_398151
Anti-EEA1	BD Bioscience	Cat# 610456; RRID: AB_397829
Biological Samples		
Human Peripheral blood mononuclear cell	SAILY BIO	Cat# SLB-HP100B

(*Continued on next page*)

Continued

REAGENT or RESOURCE	SOURCE	IDENTIFIER
Chemicals, Peptides, and Recombinant Proteins		
Recombinant human IL-2	Novoprotein	Cat# GMP-CD66
TransIT-LT1	Mirus Bio	Cat# 2300
Human T-Activator CD3/CD28 Dynabeads	Life Technologies	Cat# 11132D
MitoSOX Red Mitochondrial Superoxide indicator	Invitrogen	Cat# M36008
Paraformaldehyde	Meilunbio	Cat# MA0192
Brefeldin A	Biolegend	Cat# 420601
MYC Agarose beads	Sigma-Aldrich	Cat# A7470
N-ethylmaleimide	Sigma-Aldrich	Cat# E3876
Protease Inhibitor Cocktail	Thermo Scientific	Cat# A32953
LysoTracker Red	Invitrogen	Cat# L7528
MitoTracker Orange	Invitrogen	Cat# M7510
MG132	Selleck	Cat# S2619
NH_4Cl	Sigma-Aldrich	Cat# 254134
Cycloheximide	Cell Signaling Technology	Cat# 2112
Proteinase K	Yeasen	Cat# 10401ES60
PrimerScript RT Master Mix	TaKaRa	Cat# 10236505
TB Green Premix Ex Taq	TaKaRa	Cat# 10236504
OCT compound	SAKURA	Cat# 4583
Critical Commercial Assays		
Gibson Assembly Master Mix	New England Biolabs	Cat# E2611
Human T Cell Enrichment Kit	Stem Cell Technology	Cat# 19051
Mitochondrial Membrane Potential Assay Kit	Cell Signaling Technology	Cat# 13296
Zombie Violet Fixable viability Kit	Biolegend	Cat# 423114
CellTrace Violet Cell Proliferation Kit	Invitrogen	Cat# C34557
RNeasy Mini Kit	QIAGEN	Cat# 74104
Experimental Models: Cell Lines		
Lenti-X 293T cells	TakaRa	Cat# 632180
Jurkat E6.1 T cells	Arthur Weiss	N/A
K562 myelogenous leukemia cells	ATCC	Cat# CCL-243
EL4 lymphoma cells	ATCC	Cat# TIB-39
$Meso^+K562$	This paper	N/A
$CD19^+K562$	This paper	N/A
$Luci^+Red^+CD19^+K562$	This paper	N/A
Experimental Models: Organisms/Strains		
Mouse: NOD/SCID/Il2rg-null (B-NSG) mice	Biocytogen	Cat# 110586
Oligonucleotides		
Bcl-xL qPCR; F: 5′-GAGCTGGTGGTTGACTTTCTC; R: 5′-TCCATCTCCGATTCAGTCCCT	This paper	N/A
Bfl1 qPCR; F: 5′-TACAGGCTGGCTCAGGACTA; R: 5′-CGCAACATTTTGTAGCACTC	This paper	N/A
TFAM qPCR; F: 5′-GATGCTTATAGGGCGGAGTG; R: 5′-AGCTTTTCCTGCGGTGAATC	This paper	N/A

(*Continued on next page*)

Continued

REAGENT or RESOURCE	SOURCE	IDENTIFIER
MT-CO1 qPCR; F: 5′-ATACCAAACGCCCCTCTTCG; R: 5′-TGTTGAGGTTGCGGTCTG	This paper	N/A
NRF1 qPCR; F: 5′-AGGAACACGGAGTGACCC; R: 5′-TATGCTCGGTGTAAGTAGCC	This paper	N/A
NRF2 qPCR; F: 5′-TCCCAGCAGGACATGGATTTG; R: 5′-TGTGGGCAACCTGGGAGTAG	This paper	N/A
CAR qPC; F: 5′-TCCTGCCCCTACCATTGCTA; R: 5′-CAGTACAGCGTAATCACCAG	This paper	N/A
18S rRNA qPCR; F: 5′-CAGCCACCCGAGATTGAGCA; R: 5′-TAGTAGCGACGGGCGGTGTG	This paper	N/A
Recombinant DNA		
pHR_PGK	Addgen	Cat# 79120
pCMVdR8.92	Addgen	Cat# 8455
pMD2.G	Addgen	Cat# 12259
pHR_hCD19	This paper	N/A
pHR_hMeso	This paper	N/A
pHR_luciferase	This paper	N/A
pHR_TRAF2-mCherry	This paper	N/A
CAR.19ζ^{WT}	This paper	N/A
CAR.19ζ^{KR}	This paper	N/A
CAR.19BBζ^{WT}	This paper	N/A
CAR.19BBζ^{KR}	This paper	N/A
CAR.1928ζ^{WT}	This paper	N/A
CAR.1928ζ^{KR}	This paper	N/A
CAR.GD2BBζ^{WT}	This paper	N/A
CAR.GD2BBζ^{KR}	This paper	N/A
CAR.GD2-28ζ^{WT}	This paper	N/A
CAR.GD2-28ζ^{KR}	This paper	N/A
Software and Algorithms		
FlowJo v10	Tree Star	https://www.flowjo.com/
Amersham Imager 600 analysis software	GE	N/A
ImageJ	NIH	https://imagej.nih.gov/ij/download.html
Living Image v4.5.2 (IVIS imaging)	Perkin Elmer	N/A
GraphPad Prism 8	GraphPad	https://www.graphpad.com

RESOURCE AVAILABILITY

Lead Contact

Further information and requests for resources and reagents may be directed to and will be fulfilled by the Lead Contact, Haopeng Wang (wanghp@shanghaitech.edu.cn).

Materials Availability

Unique reagents and cell lines generated in this study may be made available on request (pending continued availability) from the Lead Contact with a completed Materials Transfer Agreement.

Data and Code Availability

The published article includes all datasets analyzed during this study.

EXPERIMENTAL MODEL AND SUBJECT DETAILS

Cell lines and cell culture

Lenti-X 293T cells (TaKaRa #632180) were used to produce lentivirus in this study. Jurkat T cells (a gift from A. Weiss at UCSF) were stably transfected with CAR-expressing lentivirus for *in vitro* assays. K562 myelogenous leukemia cells (ATCC #CCL-243) were lentivirally transduced with the full length human CD19 gene ($CD19^+$K562) as the target cells for the CD19 CAR-T cells. Meanwhile, K562 cells were engineered to stably express human mesothelin protein ($Meso^+$K562) as the control cell line. EL4 lymphoma cells (ATCC #TIB-39) were used as the target cells for the GD2 CAR-T cells. $CD19^+$K562 cells were further stably transduced with mCherry and luciferase ($Luci^+Red^+$ $CD19^+$K562) for *in vivo* tumor model of the CAR-T cells. Lenti-X 293T cells were cultured in DMEM medium supplemented with 10% FBS, 100 U/mL penicillin and 100 μg/mL streptomycin. Suspension cells were cultured in RPMI-1640 medium supplemented with 10% FBS, 100 U/mL penicillin and 100 μg/mL streptomycin. Both medium and all supplements were purchased from Thermo Scientific. All engineered cell lines were sorted with FACSAria II (BD bioscience) and examined by PCR to ensure free of mycoplasma contamination.

Mouse studies

To generate the *in vivo* tumor model, we used 5- to 8-week-old male and female NOD/SCID/Il2rg null (B-NSG) mice (from Beijing Biocytogen). NSG mice were housed in the Animal Facility at the National Facility for Protein Science in Shanghai. All mouse experiments were conducted in accordance with Shanghai Institutional Animal Care and Use Committee (IACUC) guidelines and under an approved IACUC protocol of ShanghaiTech University.

METHOD DETAILS

Constructs of chimeric antigen receptors

CARs targeting human CD19 or GD2 were used in this study. Briefly, the CAR comprised a scFv fragment, FMC63 or 14 g2a, specific for human CD19 and GD2 antigen respectively (Nicholson et al., 1997; Rossig et al., 2001) preceded by a CD8α signal peptide (Uniprot: P01732-1, aa 1-21) with a myc-tag (EQKLISEEDL) and followed by the CD8α hinge-transmembrane region (Uniprot: P01732-1, aa 138-206) and a human CD3ζ intracellular domain (Uniprot: P20963-1, aa 52-164) with or without the cytoplasmic region of human 4-1BB (Uniprot: Q07011, aa 214-255) or CD28 (Uniprot: P10747-1, aa 180-220) costimulatory domain. CARs were cloned into a modified pHR-PGK vector (Addgene #79120) via Gibson assembly cloning (NEB #E2611L), in which the PGK promoter was replaced by the hEF1α promoter and an IRES-EGFP cassette was introduced into the constructs as a reporter. In certain cases, CARs were fused with EGFP directly for imaging detection.

Human T cell culture and lentiviral transduction

Human PBMCs were isolated from peripheral blood of healthy donors by density gradient centrifugation with Human T Cell Enrichment Kit (Stem Cell Technology #19051). Human T cells were cultured in RPMI-1640 medium supplemented with 10% FBS, 100 U/mL penicillin, 100 μg/mL streptomycin, and 100 U/mL recombinant hIL-2 (novoprotein). Lenti-X 293T cells were transfected with CAR expression vector plasmid and viral packaging plasmids, pCMVdR8.92 (Addgene #8455) and pMD2.G (Addgene #12259) via TransIT-LT1 transfection reagent (Mirus #2300). 60 h post transfection, viral supernatant was harvested, concentrated by ultracentrifugation and frozen in aliquots at –80°C before use. Human T cells were stimulated with Human T-Activator CD3/CD28 Dynabeads (Life Technologies #11132D) at a bead-to-cell ratio of 3:1 for 24 h before viral infection. T cells were exposed to virus for 18 h then replaced with fresh medium. Dynabeads were removed after stimulation for 5 days. Medium and IL-2 were refreshed every 2-3 days.

Flow cytometry

For surface staining, cells were incubated with antibodies at 4°C for 25 min in FACS buffer (PBS + 2% FBS). For mitochondrial membrane potential staining, cells were incubated with 200 nM mitochondrial specific dye TMRE (CST #13296) at 37°C for 15 min. For staining of activation induced ROS, CAR-T cells were incubated with target cells at 37°C for indicated time, then mitochondrial specific ROS dye MitoSOX (Invitrogen #M36008, 5 μM final concentration) was added to the medium 15 min before harvest. For intracellular staining, cells were first fixed with 4% paraformaldehyde (Meilunbio #MA0192) at room temperature for 15 min, then permeabilized with pre-cold Methanol and incubated on ice for 50 min. The following staining was conducted at room temperature for 60 min in dark. Live/dead staining was performed using Zombie Violet Fixable viability Kit (Biolegend #423114) prior to fixation. For intracellular cytokine detection, CAR-T cells were co-cultured with target cells in the presence of Brefeldin A (Biolegend #420601) for the last 6 h. FACS data were acquired through BD LSRFortessa (BD bioscience) and analyzed by FlowJo software (Tree Star). The FACS antibody information were summarized in the Key Resources Table.

Immunoprecipitation and western blotting

Immunoprecipitation and immunoblotting of the CAR was performed using anti-Myc Agarose beads (Sigma #A7470) and anti-Myc mAb (Clone#: 9B11), respectively. For detection of CAR ubiquitination, cells were lysed with lysis buffer containing 50 mM Tris-HCl (pH 7.5), 1% Triton X-100, 200mM NaCl, 1mM EDTA, 0.2% SDS, 10mM N-ethylmaleimide (Sigma #E3876), and Protease Inhibitor Cocktail (Thermo Scientific #A32953). To isolate the endosomes of T cells, plasma membrane was mechanically broken via a 22-G needle in a homogenization buffer containing 250 mM sucrose, 3 mM imidazole, Protease Inhibitor Cocktail, 1mM Na_3VO_4, 1mM

EDTA, and 0.03 mM CHX. The homogenized cells were first centrifuged at 2000 g for 10 min at 4°C to remove nuclear pellet. The supernatant was then fractionated by gradient centrifugation in sucrose solutions with a series of density, the bottom solution containing supernatant with 41% sucrose, overlaid sequentially with 35%, 25% sucrose solution and with homogenization buffer to fill up the rest of the ultracentrifuge tube. After centrifuge at 210000 g for 2 h at 4°C, endosomes were harvest from the interphase between 35% and 25% sucrose solution.

Antibodies against the following proteins were used: Ubiquitin (Clone#: P4D1), p62 (Clone#: 3/P62 LCK LIGAND), TRAF2 (Clone#: C192), THEMIS (CST #4482), p85 (Clone#: 19H8), LAT (Clone#: E2U6J), LAT pY^{191} (CST #3584), NDUFB8 (Clone#: 20E9DH10C12), TFAM (Clone#: D5C8), Tom20 (Clone#: F-10), GAPDH (Clone#: 6C5), α-tubulin (Clone#: DM1A), ZAP-70 (Clone#: 99F2), GFP (Clone#: 7G9). Rab5 (Clone#: C8B1) was used as a loading control of endosome fraction. Chemiluminescence was performed using Amersham Imager 600 (GE). Protein quantification was achieved by using Amersham Imager 600 analysis software (GE) and normalized to loading control.

Immunofluorescence

For the tumor infiltrating CAR-T cells detection, a fraction of tumor tissues were fixed in 4% paraformaldehyde, then dehydrated in 30% sucrose and embedded in OCT compound (SAKURA #4583) followed by cryosection generation on a cryostat (Leica). Images were collected using 20 × objective of the TCS SP8 STED microscope (Leica). The imaging of lysosome and mitochondrial in CAR-T cells was performed in living cells using LysoTracker Red (Invitrogen #L7528) and MitoTracker Orange (Invitrogen #M7510). For imaging analysis of CAR-EGFP and lysosomes, CAR-T cells were first co-incubated with CD19$^+$ K562 cells for 30 min. For imaging analysis of CAR-EGFP and mCherry-TRAF2 within the early endosomes, CAR-T cells were fixed using 4% paraformaldehyde and permeabilized with 0.1% Triton X-100 in PBS containing 1% BSA. Early endosome was labeled using anti-EEA1 antibody (BD Bioscience #610456). Images of cell samples were acquired by A1R-si (Nikon) or TCS SP8 STED microscope with 60 × and 63 × oil immersion objective. Captured images were analyzed with ImageJ software (NIH).

CAR downmodulation assay

For the short-term (within one h) assays, CAR-T cells and target cells were co-incubated in a 96-well PCR plate at the ratio of 1:3 on ice. The samples were spun down for 1 min at 4°C to force the contact of two types of cells. The reaction was performed in a 37°C water bath and ended with 4% paraformaldehyde fixation. For the long-term (up to 3 days) test, two types of cells were co-cultured in a 24-well plate at 37°C and harvested at indicated time points for FACS analysis. The surface level of CAR was detected by staining anti-Myc tag antibody.

CAR degradation assay

The degradation test within one h was conducted using the same process as in short term CAR downmodulation assay except further permeabilization for intracellular staining. FACS based CAR degradation pathway test was performed in 96 U-bottom well plate at the E:T ratio of 1:3 for 8 h. MG132 (Selleck #S2619) or NH_4Cl (Sigma #254134) was added into the co-culture medium at indicated dosage to inhibit the proteasome or lysosome function. CAR-T cells and target cells were co-cultured in 48-well cell culture plate at the E:T ratio of 1:1 and harvested at indicated time points to make lysate for western blot based degradation analysis,. In some cases, 25 μg/mL Cycloheximide (CST #2112) was added to inhibit *de novo* CAR synthesis.

CAR internalization and recovery assay

Internalization assay. CAR-T cells were pre-cold on ice for 30 min and resuspended in ice-cold RPMI-1640 medium with or without 10 μg/mL Brefeldin A. Then, CAR-T cells were plate in 37°C for indicated time. Finally, 4% paraformaldehyde was added to stop reaction and fixed the CAR level for flow cytometry analysis.

Recovery assay. CAR-T cells were co-incubated with CD19$^+$ K562 cells in 96 U-bottom well plate at the E:T ratio of 1:2 for 12 h. Then cells were washed with PBS twice and resuspended in 0.1mg/mL proteinase K (Yeasen #10401ES60) at 37°C for 3 min. Cells were washed twice with medium and replated in medium with 100 μM CHX. Cell surface CAR was monitored by flow cytometry every 12 h.

FACS-based *in vitro* killing assay

Briefly, the CD19$^+$ mCherry$^+$K562 cells and MESO$^+$ mCherry$^-$ K562 cells were mixed at a ratio of 1:1 then co-incubated with CAR-T cells or non-transduced T cells at indicated E:T ratios. Control samples containing only mixed K562 cells were conducted to set FACS gating for intact living K562 cells. T cells were also stained with CD3ε to distinguish from K562 cells population. A ratio of the surviving mCherry$^+$ K562 cells and mCherry$^-$ K562 cells was calculated to evaluate the cytotoxicity of CAR-T cells. In short term killing assay, cells were seeded in 96 U-bottom well plate without IL-2 supplement overnight. For long time comparison, cells were co-cultured in 24-well plate with 50 U/mL IL-2 addition for 3 days.

In vitro proliferation assay

To start, 1 × 10^6 CAR-T cells were co-cultured with 3 × 10^5 irradiated CD19$^+$K562 cells in 24-well plates. Every 8-10 days, irradiated target cells were added with the same cell ratio as before to sustain stimulation of CAR-T cells. CAR-T cell number was counted every 2 days and complete human T cell medium was refreshed to reached a concentration of 1 × 10^6 T cells per ml meanwhile. For the FACS based proliferation assay, CAR-T cells were rested in medium without IL-2 for 24 h. The rest CAR-T cells (1 × 10^6 cells) were

then stained with 5 μM CellTrace Violet according to the protocol of CellTrace Violet Cell Proliferation Kit (Invitrogen) and coculture with irradiated $CD19^+$ K562 cells for 4 days. The fluorescent intensity of pre-labeled dye was detected by flow cytometry and proliferation index of CAR-T cells was quantified using FlowJo software.

Metabolic analysis

After stimulated with irradiated target cells for 14 days, mitochondrial function of CAR-T cells was assessed with the extracellular flux analyzer XF24 (Seahorse Bioscience). CAR-T cells were suspended in XF assay medium containing 2 mM L-glutamine, 5.5 mM glucose, and 1 mM sodium pyruvate then seeded at 1.5×10^5 cells per well. CAR-T cells were adhered to poly-L-lysine coated plate after incubation in standard culture conditions for 30 min, thenswitched to a CO_2-free incubator during instrument calibration. Cellular OCRs were measured under basal conditions following treatment with 1 μM oligomycin, 2 μM FCCP, and 40 nM rotenone with 1 μM antimycin A (Seahorse Bioscience).

Real-time PCR

CAR-T cells were stimulated with $CD19^+$K562 cells for indicated time then sorted for RNA extraction. Total RNA was extracted using the RNeasy Mini Kit (QIAGEN #74104) and reverse transcribed into cDNA using PrimerScript RT Master Mix (TaKaRa #10236505). Real-time PCR reactions were performed with TB Green Premix Ex Taq (TaKaRa #10236504) by three times paralleled replicates on a QuantStudio 7 Flex Real-Time PCR System (Applied Biosystems) based on the manufacture instructions. The expression level of each indicated gene was normalized to the housekeeping gene, Ribosomal 18S. The qPCR primer sequences were summarized in the Key Resources Table.

Mass spectrometry

CAR-T cells were co-cultured with $CD19^+$K562 cells for 5 min before lysed as the reaction sample. In ths control samples, CAR-T cells and $CD19^+$K562 cells were separately lysed and then mixed together. The protein lysates were immunoprecipitated by anti-Myc beads then separated by SDS–PAGE. The gel bands of CAR protein were cut for in-gel digestion. Briefly, the gel fragments were washed with 50 mM ammonium bicarbonate and shrunk with 50% acetonitrile, 25 mM ammonium bicarbonate. The proteins in the gel were reduced by treating DTT and alkylated by using iodoacetamide, respectively. Then, the gel was digested with trypsin in 37°C overnight. The resulted peptides were eluted with 25 mM ammonium bicarbonate and 5% formic acid, 50% acetonitrile, respectively. The eluted peptide samples were lyophilized to dryness and then desalted with C18 StageTip before LC-MS/MS analysis.

The obtained peptide samples were analyzed by an Orbitrap Fusion mass spectrometer coupled with an Easy-nLC 1000 (Thermo Fisher Scientific) ultrahigh pressure liquid chromatography pump. The LC separation system consisted of a trap column (100 μm i.d. × 4 cm) and an analytical column with integrated spray tip (75 μm i.d. × 20 cm) both packed with 3 μm/120 Å ReproSil-Pur C18 resins (provided by Dr. Maisch GmbH, Ammerbuch, Germany). The buffers used for separation were 0.1% (v/v) FA in water and 0.1% (v/v) FA in ACN. Half of the obtained samples were first loaded onto the trap column and then separated by the analytical column at a flow rate of 300 nL/min with 80 min gradient. Full MS scans were performed in the Orbitrap mass analyzer over m/z range of 350−1550 with a mass resolution of 120000. The MS/MS spectra were acquired in data-dependent mode with a Top Speed method (3 s). Tandem MS was performed in the ion trap mass analyzer using an isolation window of 1.6 Da by quadrupole mass analyzer and HCD fragmentation with normalized collision energy of 30.

The raw files were compared against the Human fasta database by MaxQuant (version 1.5.5.1). The oxidation (M), deamidation (NQ), and Glygly (K) were selected as the variable modifications for the ubiquitination peptide identification while the carbamidomethyl as the fixed modification. The maximum missed cleavage for trypsin digestion was set to 2. Label-free quantification (LFQ) and match between runs were set. Other parameters were set as default.

Xenograft Mouse Models

1×10^6 $CD19^+$ K562 FFluc cells were subcutaneously injected into the right flank of NSG mice, followed 4 days later by adoptive cell transfer of 5×10^5 non-transduced T cells or T cells expressing CAR^{WT} or CAR^{KR}. Tumor growth was monitored by bioluminescence imaging using the IVIS spectrum imaging system (Perkin Elmer) every week. Quantitative image data was acquired through Living Image Software (Perkin Elmer).

Mitochondrial Function Analysis

For mitochondrial membrane potential analysis, CAR-T cells were stained with mitochondrial specific dye TMRE (200 nM) at 37°C for 15min and then analyzed by FACS. For measuring ROS level in CAR-T cells, CAR-T cells were stimulated with target cells for indicated time, and then stained with mitochondrial specific ROS dye MitoSOX (5 μM) at 37°C for 15min followed by FACS analysis.

QUANTIFICATION AND STATISTICAL ANALYSIS

Statistical significance was determined by two tailed Student's t test. P value < 0.05 was considered statistically significant. All error bars of experimental data are presented as SEM. Statistical analysis and curve fitting was performed with Prism 8 software (GraphPad).